A high-throughput cytotoxicity screening platform reveals *agr*-independent mutations in bacteraemia-associated *Staphylococcus aureus* that promote intracellular persistence

Abderrahman Hachani[1, #,*], Stefano G. Giulieri[1,#], Romain Guérillot[1,#], Calum J. Walsh[1], Marion Herisse[1], Ye Mon Soe[1], Sarah L. Baines[1], David R. Thomas[1], Shane Cheung[2], Ashleigh S. Hayes[1], Hyun-Jung Cho[2], Hayley J. Newton[1,3], Sacha Pidot [1], Ruth C. Massey[4,5,6,7], Benjamin P. Howden[1,8,§], and Timothy P. Stinear[1, §].

1. Department of Microbiology and Immunology, Doherty Institute, University of Melbourne, Melbourne, Victoria, 3000, Australia
2. Biological Optical Microscopy Platform, University of Melbourne, Melbourne, Victoria, 3000, Australia
3. Infection and Immunity Program, Department of Microbiology and Biomedicine Discovery Institute, Monash University, Clayton, VIC, Australia.
4. School of Microbiology, University College Cork, Cork, Ireland.
5. School of Medicine, University College Cork, Cork, Ireland.
6. APC Microbiome Ireland, University College Cork, Cork, Ireland.
7. School of Cellular and Molecular Medicine, University of Bristol, Bristol, UK
8. Microbiological Diagnostic Unit Public Health Laboratory, Department of Microbiology and Immunology, Doherty Institute, University of Melbourne, Melbourne, Victoria, 3000, Australia

Joint first author

§ Joint senior author

*Corresponding author: Abdou Hachani abderrahman.hachani@unimelb.edu.au

Keywords: *Staphylococcus aureus*, cytotoxicity, bacterial population genomics, evolutionary convergence analysis, GWAS, quorum sensing, pathogenesis, intracellular

Abstract

Staphylococcus aureus infections are associated with high mortality rates. Often considered an extracellular pathogen, *S. aureus* can persist and replicate within host cells, evading immune responses and causing host cell death. Classical methods for assessing *S. aureus* cytotoxicity are limited by testing culture supernatants and endpoint measurements that do not capture the phenotypic diversity of intracellular bacteria. Using a well-established epithelial cell line model, we have developed a platform called *InToxSa* (Intracellular Toxicity of *S. aureus*) to quantify intracellular cytotoxic *S. aureus* phenotypes. Studying a panel of 387 *S. aureus* bacteraemia isolates, and combined with comparative, statistical and functional genomics, our platform identified mutations in *S. aureus* clinical isolates that reduced bacterial cytotoxicity and promoted intracellular persistence. In addition to numerous convergent mutations in the Agr quorum sensing system, our approach detected mutations in other loci that also impacted cytotoxicity and intracellular persistence. We discovered that clinical mutations in *ausA,* encoding the aureusimine non-ribosomal peptide synthetase, reduced *S. aureus* cytotoxicity and increased intracellular persistence. *InToxSa* is a versatile, high-throughput cell-based phenomics platform and we showcase its utility by identifying clinically relevant *S. aureus* pathoadaptive mutations that promote intracellular residency.

Introduction

Staphylococcus aureus is a leading cause of hospital-acquired infections, a problem exacerbated by increasing resistance to last-line antibiotics (Murray et al., 2022; Tong et al., 2015). *S. aureus* is traditionally considered an extracellular pathogen as it produces many secreted virulence factors, including superantigens, degradative enzymes and cytolytic toxins (Tam & Torres, 2019). The potent pore-forming toxins (PFTs), including alpha-hemolysin and leukocidins, are among the major virulence determinants of *S. aureus* (Cheung et al., 2021). These toxins induce rapid host cell death, including death of the leukocytes and neutrophils recruited to remove bacteria from infected tissues (Surewaard et al., 2016; Thammavongsa et al., 2015).

Long-term asymptomatic *S. aureus* carriage is common but invasive infection is rare. Thus, understanding the changes enabling *S. aureus* to switch from a common coloniser of the nasal cavity to an invasive pathogen is a major research focus. A powerful discovery approach has been used to compare the cytolytic activities of secreted *S. aureus* virulence factors between colonising and bacteraemia isolates, followed by genomics to uncover the bacterial genetic loci linked with high/low cytolytic activity (Collins et al., 2008; Giulieri et al., 2018; Laabei et al., 2014, 2021; McConville et al., 2022). These toxicity analyses use methods that monitor eukaryotic cell viability upon exposure to *S. aureus* culture supernatants (Dankoff et al., 2020; Das et al., 2016; Giulieri et al., 2018) and integrate these phenotypes within genome wide association studies (GWAS) and other comparative bacterial population genomics techniques (Giulieri et al., 2018; Recker et al., 2017). However, such toxicity assays are limited in that they focus on exogenous virulence factors that have accumulated in the culture media during bacterial growth. Thus, such methods can be limiting as they report phenotypes that are temporally skewed and ignore the host cell-bacterium context under which the production of these factors is controlled during infection. When these endpoint toxicity assays are conducted at scale with many hundreds of bacterial isolates, additional

77 issues caused by filter-sterilisation, freeze-storage and other manipulations during the preparation
78 of bacterial supernatants prior to incubation with host cells may increase assay variability (Giulieri
79 et al., 2018; McConville et al., 2022).
80
81 Another restriction of toxicity assays is that they treat *S. aureus* as an obligate extracellular
82 pathogen, whilst the literature has reported its capacity to adopt an intracellular behaviour, readily
83 adhering to and invading various eukaryotic cells, including non-professional phagocytes (Flannagan
84 et al., 2016; Foster et al., 2014; Soe et al., 2021). Upon internalisation, intracellular *S. aureus* initially
85 reside in phagolysosomes, where low pH is a cue for bacterial replication (Flannagan et al., 2018;
86 Lâm et al., 2010). *S. aureus* uses its arsenal of PFTs to escape from this degradative compartment,
87 into the cytosol and cause the death of host cells (Moldovan & Fraunholz, 2019; Siegmund et al.,
88 2021). This intracellular niche confers protection to *S. aureus* from antibiotics and immune
89 responses (Peyrusson et al., 2020; Strobel et al., 2016). While guarding *S. aureus* from host attack,
90 intracellular residency also enables the creation of a reservoir for the pathogen to persist in an
91 infected host and could lead to bacterial transmigration into distal host tissues, from where the
92 bacteria can cause protracted infections and more serious disease (Jorch et al., 2019; Surewaard et
93 al., 2016). Toxicity and persistence of *S. aureus* in an intracellular context are critical pathogenesis
94 traits. However, understanding these traits and their microevolution across diverse collections of
95 clinical *S. aureus* strains, and correlating them with specific bacterial genetic variations has been
96 hampered by the lack of a high-throughput platform for trait characterisation.
97
98 To address these issues, we took advantage of the capacity of *S. aureus* to invade cultured epithelial
99 cell lines and established a 96-well assay format to accurately monitor over time the bacterial
100 toxicity exerted from within host cells. HeLa cells are adherent epithelial cells and represent an
101 amenable model to study the pathogenesis of most intracellular bacteria causing human disease,

including *S. aureus* (Das et al., 2016; Stelzner, Hertlein, et al., 2020; Stelzner, Winkler, et al., 2020). We modified an antibiotic/enzyme protection assay, using a combination of gentamicin and lysostaphin, to kill extracellular bacteria while preserving the viability of intracellular bacteria (Kim et al., 2019). Using propidium iodide as a marker of host cell death, the assay measured changes in fluorescence of HeLa cells over time caused by the presence of intracellular *S. aureus*. Combined with the power of bacterial genomics and evolutionary convergence analysis, we used the assay to screen a large collection of *S. aureus* bacteraemia isolates. Our large-scale pheno-genomics approach revealed known and previously undescribed loss-of-function mutations that were significantly associated with reduced intracellular cytotoxicity and increased intracellular persistence.

RESULTS

InToxSa assay development.

We set out to develop a high-throughput and continuous cell death assay that could measure the intracellular toxicity of *S. aureus* in a format we named *InToxSa*. We used adherent HeLa-CCL2 epithelial cells as an infection model in a 96-well format and infected them with *S. aureus* at a standardised multiplicity of infection (MOI). Following an infection period of 2h, infected cells were treated with an antibiotic/enzyme combination to specifically kill extracellular bacteria and prevent further reinfection by bacteria released by cells dying during the assay. HeLa cell viability was continuously monitored by measuring propidium iodide (PI) fluorescence (see methods). Reduced HeLa cell viability was indicated by increasing fluorescence over time (Figure 1A). We used regression to fit standardised curves to the PI uptake data and calculated seven kinetic parameters including the area-under-the-curve representing the total of PI uptake over time [AUC], peak PI

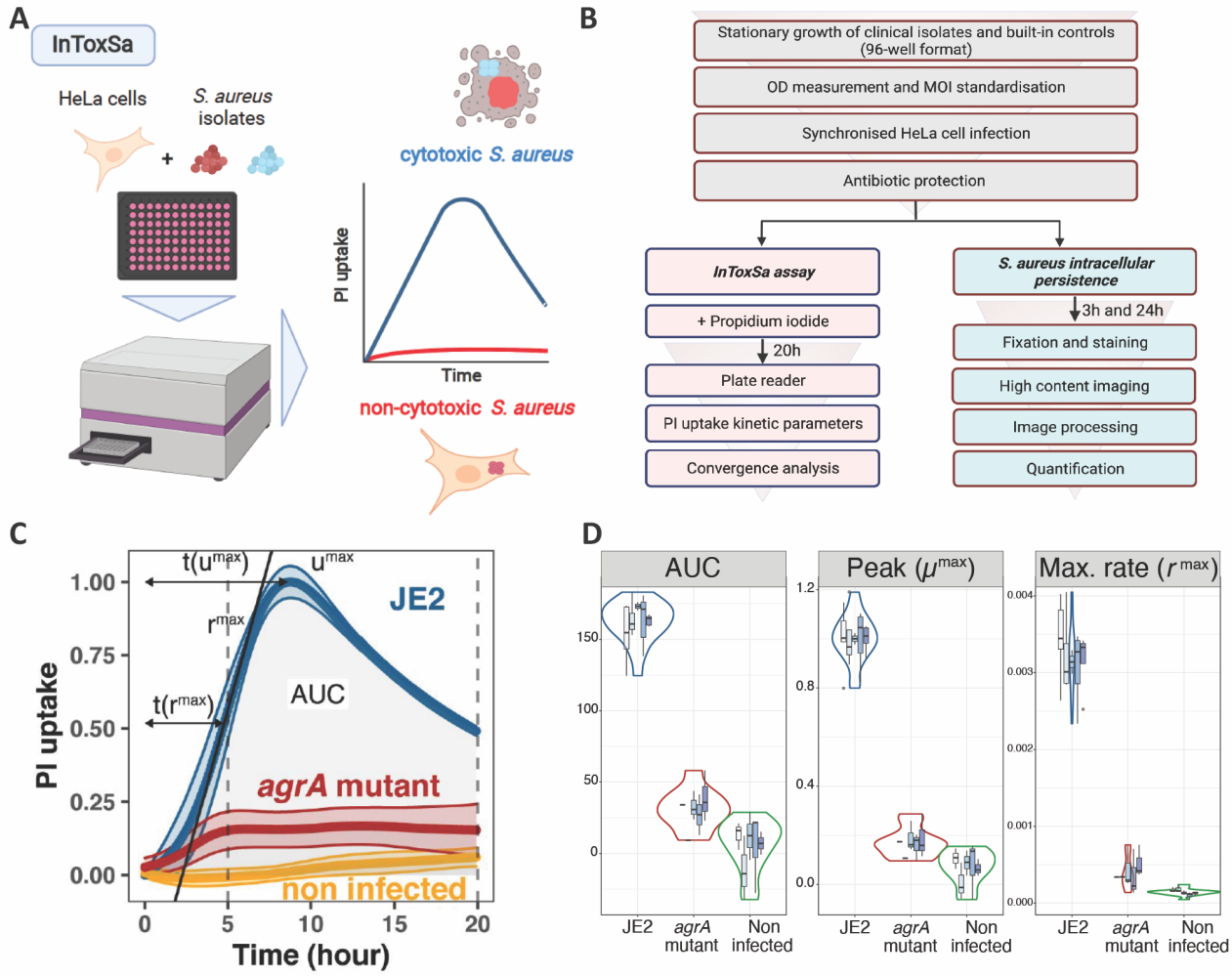

Figure 1: Establishing the intracellular toxicity of S. aureus (InToxSa) assay. *(A) Overview of InToxSa assay. (B) Flow chart of the analytical pathway. (C) Plot of PI fluorescence uptake over 20h as a measure of S. aureus intracellular cytotoxicity in HeLa cells. Depicted curves are wild type S. aureus JE2 (blue), the isogenic S. aureus JE2 agrA transposon mutant (red), and uninfected cells (yellow). The PI uptake curve for JE2 is annotated with five kinetic parameters. For each curve, the thick line represents the mean and the shading, the standard deviation. Curves are fitted with cubic smooth splines (see methods). To minimise batch effect, all kinetics data have been transformed using proportion of maximum scoring (POMS) using JE2 controls as reference minimum and maximum values (Little, 2013). X-axis is time and Y-axis is PI-uptake, represented as a proportion of maximal fluorescence in JE2-infected cells, where for every measured plate, a PI uptake value of 1 represents the maximum of JE2 PI uptake and zero its minimum. (D) Summary of five independent InToxSa experiments to assess assay and parameter variation. Violin plots represent the density distribution of all five replicates and the nested box plots show the distribution of within plate replicates (3-5 technical replicates per plate replicate) for the three most discriminatory of seven parameters inferred from the PI uptake data (Supplementary file 1).*

uptake [μ^{max}], the time to μ^{max} [$t(\mu^{max})$], the maximum rate in PI uptake [r^{max}], the time to r^{max}

126 [t(r^{max})]), trough and time to trough (Supplementary file 1).

127

128 We then mapped out a series of experiments to validate *InToxSa* and explored bacterial genetic
129 factors linked to intracellular cytotoxicity (Figure 1B). To demonstrate method performance, we
130 measured the intracellular toxicity of the wild type *S. aureus* USA300 strain JE2 against an isogenic
131 *agrA* mutant (Nebraska Transposon Library mutant NE1532 (Fey et al., 2013)), using non-infected
132 cells as a baseline (Figure 1C). *S. aureus* JE2 caused a rapid and substantial increase in PI fluorescence
133 over time, reflective of the known high cytotoxicity of this strain (Das et al., 2016; Grosz et al., 2014;
134 McConville et al., 2022). Cells infected with the *agrA* mutant yielded significantly lower PI uptake
135 (AUC) and slower (r^{max}), indicating HeLa cell viability during the infection course and is consistent
136 with the reported low cytotoxicity of *S. aureus agr* mutants (Figure 1C) (Laabei et al., 2021;
137 McConville et al., 2022).

138

139 We then assessed the reproducibility and repeatability of *InToxSa* across five experimental
140 replicates, each time using both biologically independent HeLa cell culture passages and
141 independent *S. aureus* cultures with the same two comparator strains (JE2 wild type and the
142 isogenic *agrA* transposon mutant) (Figure 1C). We measured seven PI-uptake curve kinetic
143 parameters (Figure 1C, Supplementary file 1). We observed that the PI-uptake area-under-the-curve
144 (AUC), peak PI uptake [μ^{max}] and maximum PI uptake rate [r^{max}] for *S. aureus* JE2 compared to the
145 *agrA* mutant and non-infected cells were significantly different, had very low intra-assay variation,
146 and were among the most discriminatory and reproducible PI uptake curve parameters (Figure 1D,
147 Table 1, Supplementary file 1). At experimental endpoints, the acidity of the culture media had not
148 changed, and no bacterial growth was observed after plating the media from infected 96-well
149 plates, indicating that *InToxSa* assessed the cytotoxicity caused only by intracellular *S. aureus* (data
150 not shown).

Table 1: Summary of *InToxSa* assay performance

Strain	No. biological replicates	Area under the curve [AUC]		Peak uptake [μ^{max}]		Max uptake [r^{max}]	
		Mean	CoV	Mean	CoV	Mean	CoV
S. aureus JE2 wild type	25	162	0.09	1	0.09	0.003	0.13
S. aureus JE2 *agrA* mutant	11	30.90	0.45	0.17	0.35	0.0004	0.52
Non-infected	15	5.28	3.46	0.07	1.02	0.0001	0.32

Note: CoV = Coefficient of Variation

Confirmation of *S. aureus* internalisation in HeLa cells

We used confocal microscopy to confirm the presence of intracellular *S. aureus* (Figure 2A). HeLa cells grown on coverslips were infected with the same conditions used for *InToxSa* and analysed at 3h, 8h and 24h post-infection. These timepoints were selected to reflect the key *InToxSa* timepoints highlighted during JE2 infection (start of PI uptake measurement, peak PI uptake [μ^{max}] and experimental endpoint, respectively). We observed that at each timepoint, both JE2 and the *agrA* mutant co-localised with the lysosomal marker LAMP-1. However, the *agrA* mutant was detected in higher numbers within cells compared to wild type (Figure 2A, B). At later time points (8h and 24h) the number of JE2-infected cells decreased, with fewer detectable intracellular bacteria, suggesting that JE2-infected cells had died, consistent with bacterial cytotoxicity. In contrast, the number of cells infected with the *agrA* mutant did not vary significantly, indicating cell survival during the infection time course (Figure 2B). It also appeared that the number of intracellular bacteria increased for cells infected with the *agrA* mutant, suggesting bacterial replication over time. This latter observation was explored in more depth using high-content/high-throughput imaging (see

later section). The microscopy results support the *InToxSa* assay outputs and indicate that non-cytotoxic *S. aureus,* such as the *agrA* mutant, can persist within cells without affecting cell viability.

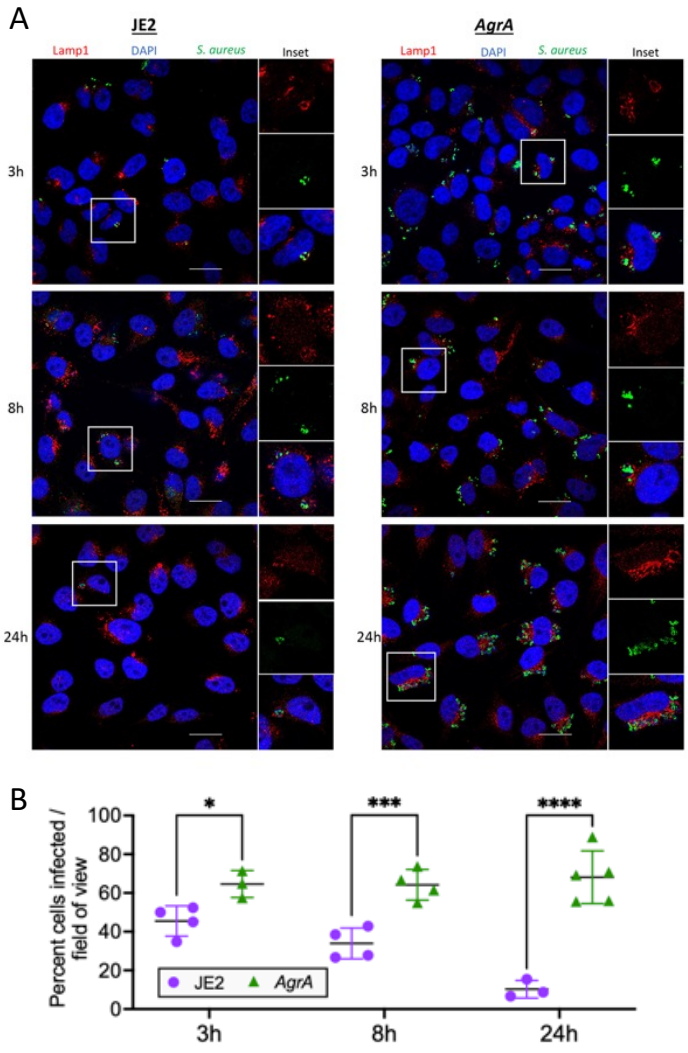

Figure 2: Fluorescence confocal microscopy of intracellular S. aureus. (A) *HeLa cells were infected with S. aureus (wild type JE2 or isogenic agrA mutant) and imaged at 3h, 8h and 24h post-infection. Fixed cells were labelled with LAMP-1, S. aureus antibodies and DAPI.* ***(B)*** *Manual quantification of confocal microscopy. Graph shows the percentage of cells infected with S. aureus at each of the three timepoints. At least 50 cells (n cells=51-112) were counted in 3-5 fields of view, with at least 12 cells counted per field (n field=12-40). Shown are all data points, mean and standard deviation. Significance was assessed using 2-way ANOVA. Null hypothesis (no difference between means) rejected for adj p<0.05. *p=0.04, ***p=0.007, ****p=<0.0001*

InToxSa benchmarking against trypan blue exclusion assay

In a previous study we used a trypan blue exclusion assay with THP1 human macrophages exposed to culture supernatants to test within-host cytotoxicity variations from 51 clinical *S. aureus* isolated from 20 patients with bacteraemia (Giulieri et al., 2018). These 51 *S. aureus* isolates were originally selected because they were associated with phenotypic changes occurring during bacteraemia, such as infection relapse, antibiotic treatment failure, longer duration of bacteraemia and augmented vancomycin MIC; phenotypes likely resulting from within-host evolution (Giulieri et al., 2018). Thus,

179 the isolates were categorised by patient and by their sequential isolation, with the first isolate
180 considered as 'baseline' and the subsequent isolates designated as 'evolved'.

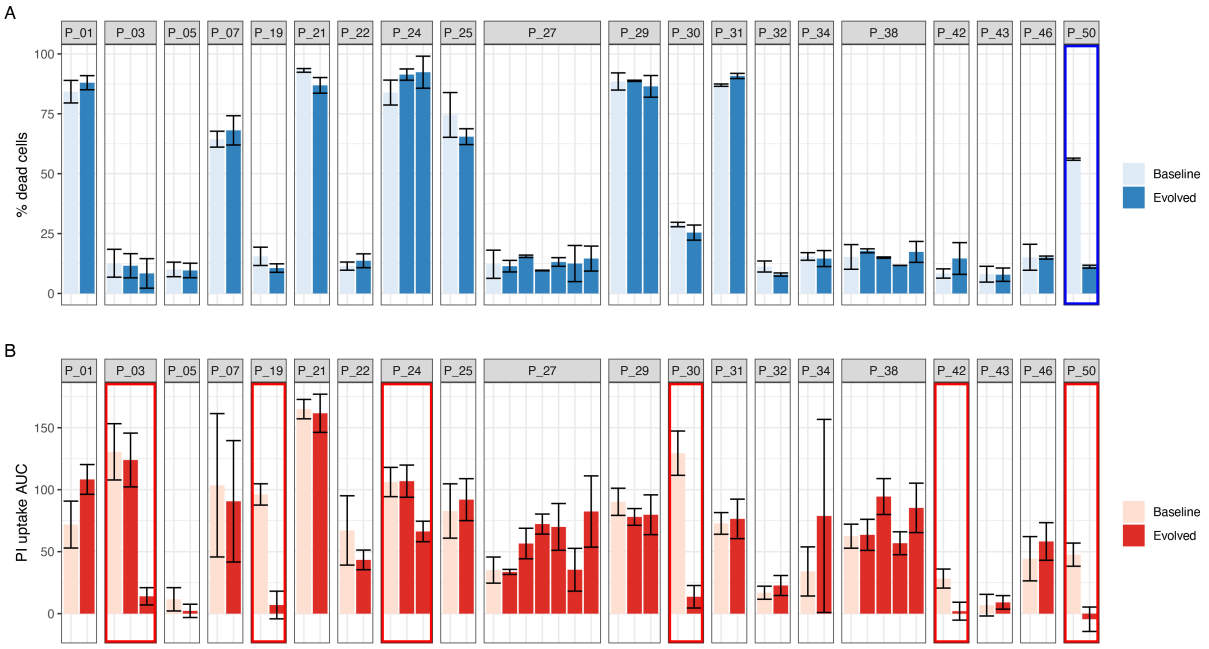

Figure 3: Performance of InToxSa against Trypan blue exclusion assay. *Comparative evaluation of S. aureus intracellular cytotoxicity with bacterial supernatants for 51 paired isolates from 20 patients with S. aureus bacteraemia.* ***(A)*** *Supernatant-based cytotoxicity on THP1 cells. Episode with significant difference in THP1 survival between baseline and evolved isolates is boxed in blue ($p<0.05$). Assay performed in biological and technical duplicates. Bars represent mean percentage of dead cells; error bars show range between duplicates. Toxicity within isolate groups was compared using analysis of the variance (ANOVA) with Bonferroni correction* ***(B)*** *PI uptake of infected HeLa cells. Values are mean AUC and standard deviation. Episodes exhibiting significant phenotypic differences between baseline and evolved isolates are boxed in red ($p<0.05$). Assay performed in biological and technical triplicates. PI uptake AUC within isolate groups was compared using ANOVA with Bonferroni correction.*

181

182 All 51 isolates were screened with *InToxSa* and compared with the original trypan blue assay data
183 (Figure 3). Using trypan blue exclusion, only the evolved isolate from patient 50 (P_50) showed a
184 significant phenotypic difference in cytotoxicity (Fig 3A). This difference was attributed to a loss-of-
185 function mutation in *agrA* (T88M). *InToxSa* also identified a significant cytotoxicity difference for
186 the P_50 isolate pair, validating the previous observation, despite the methodological and host cell

type differences. However, *InToxSa* detected significantly reduced cytotoxicity for the evolved isolates from five more patient pairs compared to the original trypan blue screen (Figure 3B). These results support the higher sensitivity of *InToxSa* in uncovering *S. aureus* cytotoxicity variations resulting from the evolution of the bacterial population during bloodstream infection.

Screening a large collection of clinical *S. aureus* to evaluate intracellular cytotoxicity

A major motivation for developing the *InToxSa* assay was to develop a pheno-genomics platform to efficiently measure the intracellular cytotoxicity profiles of a large collection of clinical *S. aureus* isolates and then use the power of comparative and statistical genomics to find bacterial genetic loci associated with intracellular cytotoxicity. To this end, we analysed 387 clinical *S. aureus* isolates, obtained from 298 episodes of bacteraemia and for which genome sequences were available (Giulieri et al., 2018; Holmes et al., 2011, 2014; VANESSA study group, on behalf of the Australasian Society for Infectious Diseases (ASID) Clinical Research Network (CRN) et al., 2018). A 164,449 SNP core genome phylogeny was inferred for this collection. The 387 isolates spanned 32 sequence types (STs) and were dominated by ST239, accounting for 30% of isolates (n:117), followed by ST22 (n:32, 8%), ST5 (n:34, 8%), ST45 (n:28, 7%), and ST1 (n:18, 5%). Fifty-three percent of the isolates were *mecA* positive (Figure 4A) (Supplementary file 3).

We assessed each of the 387 isolates by *InToxSa*, with the cytotoxicity phenotype for each isolate represented by mean PI uptake (AUC) and displayed as a heatmap, aligned with the core genome phylogeny (Figure 4A). Several patterns were readily seen in the data. There was a wide range of cytotoxicity profiles across the 387 isolates, with notable variations within each sequence type suggesting frequent adaptation events affecting intracellular cytotoxicity levels. Two sequence types (ST239 and ST22) strongly associated with lower cytotoxicity. These variations are consistent with previous observations (Laabei et al., 2021).

212 To select the most suitable *InToxSa* parameters for our statistical genomics approach, we assessed
213 their relative importance by fitting the data using unsupervised random forest (RF) machine learning
214 (Mantero & Ishwaran, 2021). In this model, 'observations' were each of the PI-uptake values for the
215 387 isolates and controls and 'features' were the seven PI uptake curve parameters (Supplementary
216 file 4). We then tested RF feature importance and showed with *variable importance plots* that the

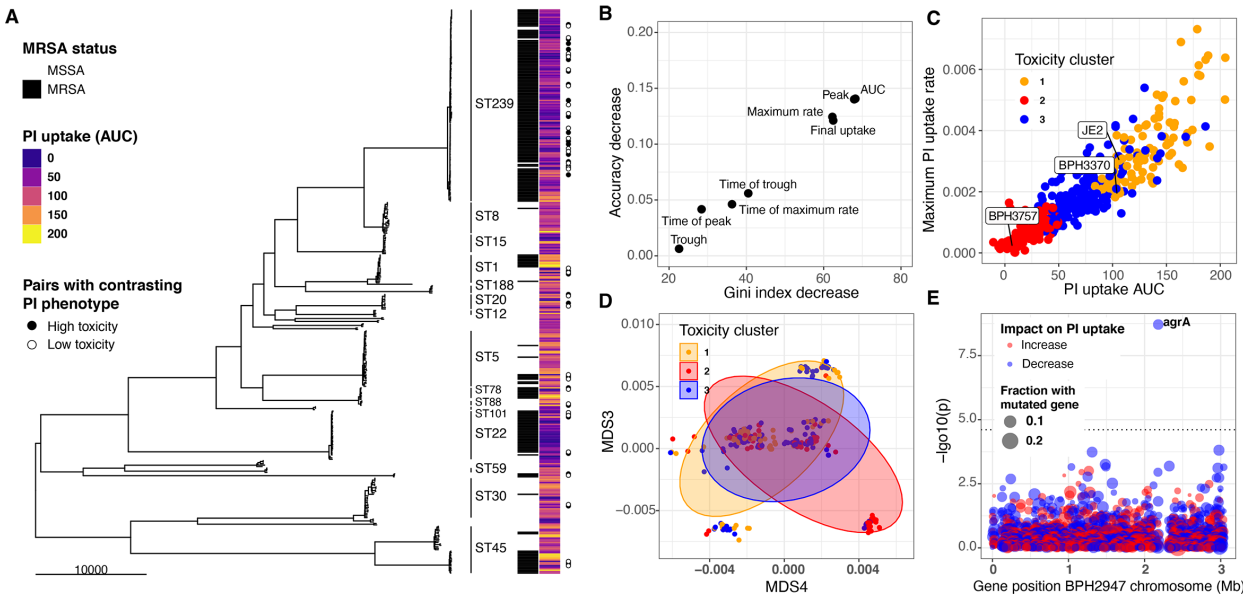

Figure 4. Intracellular cytotoxicity assessment of 387 bloodstream-associated clinical S. aureus isolates. *(A) Maximum likelihood phylogeny based on 164,449 core genome SNPs for 387 S. aureus, showing sequence type (ST) and MRSA distribution. The heatmap depicts the mean area under the curve (AUC) of cytotoxicity based on InToxSa PI uptake assay. AUC values range from non-cytotoxic (score: 0, dark blue) to highly cytotoxic (score: 200, yellow). Adjacent to the heatmap (closed and open circles) are 28 pairs of genetically related, but phenotypically discordant isolates (see Figure 5). (B) 'Variable importance plot' showing different PI uptake metrics (features) in an unsupervised random forest (RF) machine learning model. The higher the value of 'accuracy decrease' or 'Gini index decrease', the higher the importance of the feature in the model. (C) Scatter plot of the two most discriminatory PI uptake kinetic metrics (AUC and maximum PI uptake rate). Dots are coloured based on the clustering obtained from the proximity matrix of the RF model. (D) Scatter plot showing the two principal components with the strongest association with PI uptake (lineage effect as measured using pyseer). Dots and ellipses are coloured based on the clustering obtained from the proximity matrix of the unsupervised machine learning model. (E) Manhattan plot of gene-burden GWAS of cytotoxicity (PI uptake AUC) of 387 clinical isolates.*

PI uptake parameters, AUC, μ^{max} and r^{max} were the most informative features for the model (Figure 4B), consistent with our initial *InToxSa* assessment using JE2 and the *agrA* mutant (Figure 1C and 1D). Using the *proximity matrix* from the unsupervised RF model, we defined three main PI-uptake clusters, corresponding with *low*, *moderate*, and *high* intracellular cytotoxicity categories. We labelled each of the 387 PI-uptake data points with these three (*low, moderate, high*) cytotoxicity categories and plotted the AUC and r^{max} values against each other (Figure 4C). As expected, these parameters were strongly, positively correlated, suggesting that the AUC alone is sufficient to capture intracellular cytotoxicity differences between *S. aureus* isolates. We used principal component analysis (PCA) of the PI-uptake data as an alternative unsupervised learning approach (Figure 4- Supplementary Figure 1). When considering the first two components (67% of the variance explained), we observed a similar pattern where the same toxicity groups could be recognised within a cytotoxicity continuum among clinical isolates (Figure 4- Supplementary Figure 1).

GWAS analysis using *InToxSa* outputs to identify *S. aureus* genes linked to intracellular cytotoxicity

We next used GWAS to identify genetic correlates of strain-level cytotoxicity, expressed as mean PI uptake AUC. The fraction of cytotoxicity variation explained by genetic variation (heritability: h^2) was 49%, a figure lower than the ones obtained for other phenotypes such as vancomycin resistance (Giulieri, Guérillot, Holmes, et al., 2022). A lower heritability could be resulting from the *InToxSa* assay variability or caused by differences in gene expression levels or due to epigenetic changes.

To assess the contribution of lineage effects relative to locus effects, we defined lineages using multi-dimensional scaling (MDS) of a pairwise genetic distance matrix generated by Mash, a tool that reduces genome content to a set of 'sketches' (hashed k-mers) (Ondov et al., 2016). Major MDS

axes correlated with the most prevalent STs, for example ST239 was mainly defined by MDS1 (negative correlation) and MDS2 (positive correlation) (Figure 4- Supplementary Figure 3A). We then tested the association between the first 10 MDS axes (90% of the genetic variance explained) and the PI uptake phenotype in Pyseer (Earle et al., 2016; Giulieri, Guérillot, Holmes, et al., 2022; Lees et al., 2018). In agreement with the initial observations based on the phylogeny and cytotoxicity heatmap (Figure 4A), we observed significant cytotoxicity-lineage associations represented by MDS3 and MDS4 (Figure 4D, Figure 4- Supplementary Figure 2). Because of the ST-MDS lineages correlation, this is consistent with differences in cytotoxicity between clones (Figure 4- Supplementary Figure 3B). Using the three cytotoxicity clusters defined by RF as categorical labels (Figure 4C), we plotted the 387 genomes along these two dimensions. While intracellular cytotoxicity was strongly associated with some *S. aureus* lineages, this analysis showed that lineage alone does not completely explain the phenotype, as indicated by the significant overlap between the three cytotoxicity clusters across MDS3 and MDS4 (Figure 4D). This pattern is consistent with other adaptive phenotypes (Earle et al., 2016; Giulieri, Guérillot, Holmes, et al., 2022; Su et al., 2021) and suggests that locus effects from specific micro-evolutionary events modulate cytotoxicity, supporting the use of GWAS and convergent evolution approaches to identify these mutations.

Correcting for the observed population structure, we then used gene-burden GWAS to try and identify *S. aureus* loci significantly associated with intracellular cytotoxicity (PI uptake AUC) as a continuous variable. After correcting for multiple testing, only *agrA* reached the $p<0.05$ significance threshold, supporting the important contribution of this locus to strain-level cytotoxicity (Figure 4E, Supplementary file 5). We also considered the highest-ranking loci that did not reach genome-wide statistical significance. The second most significant gene, *secA2* ($p = 1.5x10-4$) encodes the accessory ATPase to the Sec protein export system and is essential for the transport of SraP, a surface exposed and serine-rich staphylococcal protein which is associated with adhesion to, and invasion of

267 epithelial cells and binding to human platelets (Siboo et al., 2005; Yang et al., 2014). Another high-
268 ranking GWAS locus was *ileS* (p=9.9x10-4), encoding an isoleucyl-tRNA synthetase linked with
269 mupirocin resistance, and previously associated with *S. aureus* cytotoxicity (Yokoyama et al., 2018).
270
271 **Identification of convergent mutations in genetic pairs with divergent *InToxSa* cytotoxicity**
272 **profiles**
273 Despite the relatively small sample size for this kind of analysis, the gene-burden GWAS detected
274 the *agrA* locus with a high significance, but it did not have sufficient power to detect mutations
275 other than the *agr* genes. We further sought to identify rare mutations that might alter the
276 intracellular cytotoxicity using comparative genomics approaches, a complementary strategy to
277 microbial GWAS (Chen & Shapiro, 2021; Giulieri, Guérillot, Holmes, et al., 2022; Saund & Snitkin,
278 2020). We used evolutionary convergence analysis to identify additional loci associated with
279 intracellular cytotoxicity among the 387 *S. aureus* isolates. Our approach was to identify genetically
280 related pairs of isolates with contrasting PI-uptake AUC values from across the phylogeny and then
281 search for homoplasic mutations between the pairs. We calculated genetic distances between all
282 387 genome-pairwise comparisons (149,769 combinations) and calculated a delta-PI uptake AUC
283 value for each pair. We selected 28 *S. aureus* pairs with a genetic distance <200 core-genome SNPs
284 and a significant decrease in PI uptake AUC between reference (isolate-1) and control (isolate-2)
285 (Wilcoxon rank-sum test) (Figure 5A). Variants within each pair (*i.e.,* found in isolate-2 but not in
286 isolate-1) were identified and annotated using a strategy that we have developed for *S. aureus*
287 within-host evolution analysis (Giulieri, Guérillot, Duchene, et al., 2022a). We have previously
288 shown that a SNP-calling approach using *de novo* assembly of one genome in a pair as a reference
289 provided the most accurate estimate of the genetic distance (Higgs et al., 2022). There were
290 between 0 – 206 mutations within the 28 pairs (Figure 5B). Mapping the genes in which these
291 mutations were found back to a core-genome phylogeny constructed from the 56 paired *S. aureus*

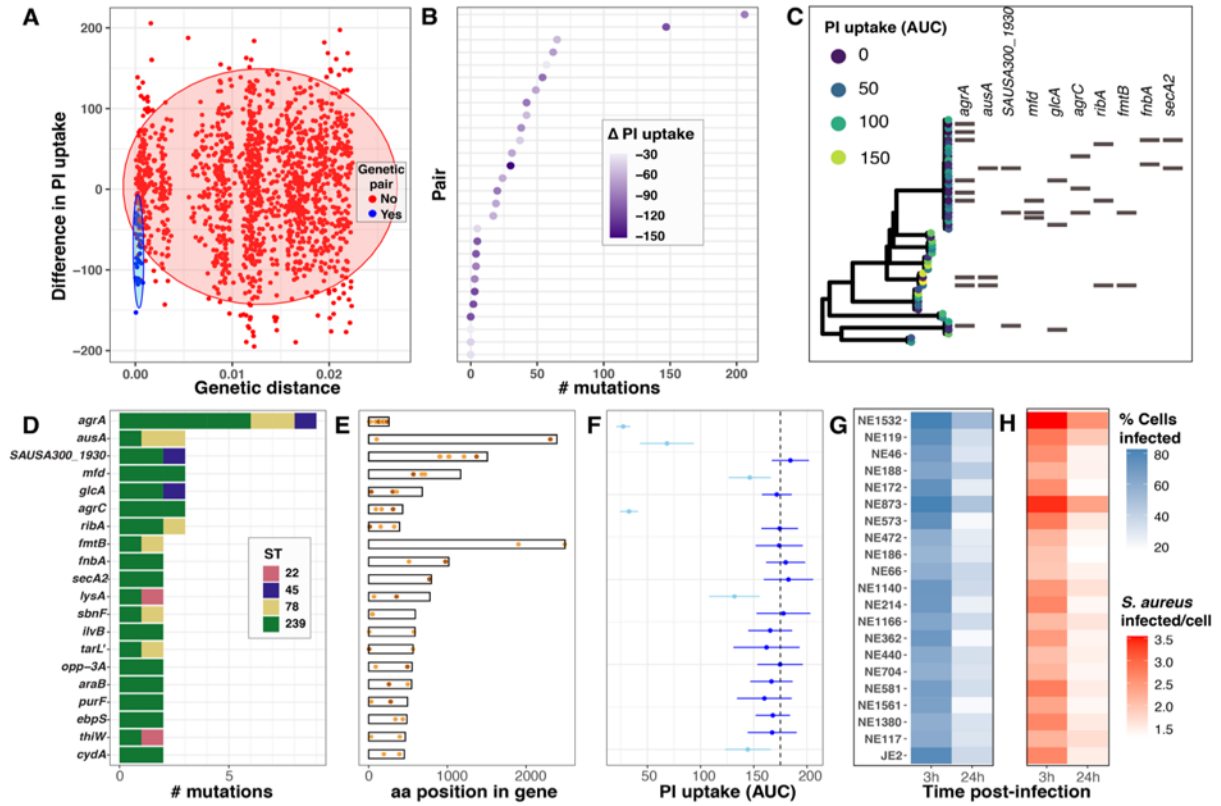

Figure 5. Evolutionary convergence analysis to identify S. aureus genes linked with intracellular cytotoxicity. *(A) Distribution of genetic distance determined by pairwise comparisons using MASH distances among the 387 S. aureus genomes, against the difference in PI uptake AUC between each pair. The shaded circles denote the 95% multivariate t-distribution (blue: pairs included in the convergence analysis; red: pairs excluded from the analysis). (B) Ranked distribution of the difference in PI-uptake AUC between the 28 pairs. Heatmap shows reduction in AUC values. (C) Core genome phylogeny for the 28 pairs of isolates. Tree tips are coloured by PI-uptake AUC. Aligned with the phylogeny, the 10 first genes targeted by convergent mutations are shown. (D) Number of mutations detected for each of the 20 genes, coloured by S. aureus ST. (E) Location of convergent mutations in each gene (non-synonymous in orange, truncating in maroon). (F). Effect of loss of function for each of the 20 genes on intracellular cytotoxicity measured by InToxSa, using mutants from the Nebraska transposon library. Dotted line shows mean PI-uptake AUC of positive control strain JE2. Depicted are mean (dot) and SD (bar) of biological triplicates. Mutants causing significantly lower PI uptake AUC to JE2 are depicted in light blue, non-significant changes are in dark blue (Wilcoxon rank-sum test, corrected for multiple testing). (G)&(H) Operetta high-content imaging analysis for each of the 20 Nebraska transposon mutants and JE2 positive control. Heat maps show the percentage of HeLa cells infected with each transposon mutant (blue) and the number of bacteria per infected cells at 3h and 24h post-infection (red).*

292 genomes showed convergent (homoplasic) mutations in *agrA*, supporting the GWAS findings, and

293 also identified potentially convergent mutations in several other genes (6 with three independent
294 mutations and 35 with two independent mutations) (Figure 5C, D, E, Supplementary file 6).
295 However, because of the strong lineage effect and the paucity of representation for some *S. aureus*
296 lineages (clonal complexes [CC] and sequence types [ST]), half of these mutations were only found
297 in ST239, a well-represented lineage in our collection. In addition to target loci dedicated to the
298 regulation of virulence factors such as the *agr* locus or involved in adhesion to host extracellular
299 matrix proteins such as fibronectin and elastin (*fnbA* and *ebpS*), some of the convergent mutations
300 were found in genes involved in metabolic processes (*ribA*, *purF*, *sbnF, ilvB, lysA, araB*), associated
301 with the cell wall (*fmtB)*, devoted to the last step of the cell wall teichoic acid biosynthesis (*tarL'*),
302 implicated in DNA repair (*mfd*), in protein transport (*secA2*), in solute transport (*glcA, opp-3A, thiW*),
303 in respiration (*cydA*) and found in a phage-associated locus (SAUSA300_1930). Aside from *agrA* and
304 *agrC* genes (Giulieri et al., 2018; Laabei et al., 2014, 2015; Mairpady Shambat et al., 2016), and those
305 found in the promoter of the *tar* locus (Brignoli et al., 2022; Laabei et al., 2014), mutations in the
306 other loci have not been associated with the reduction of cytotoxicity in clinical *S. aureus* isolates.
307 Interestingly, homoplasic mutations were also found in the gene *ausA*, known to be involved in *S.*
308 *aureus* escape from epithelial cell endosomes and the phagosome of phagocytic cells (Blättner et
309 al., 2016).
310
311 **Functional assessment of genes with convergent mutations**
312 To assess the functional consequences of the convergent mutations (caused by at least two
313 homoplasic mutations per gene), we again turned to the Nebraska transposon library and selected
314 transposon mutants for 20 genes we had identified (Figure 5D). We used *InToxSa* to assess the effect
315 of gene disruption on the intracellular cytotoxicity phenotype for each mutant compared to the JE2
316 wild type (Figure 5F). Over the 20 transposon mutants tested, six showed a statistically significant
317 reduction in cytotoxicity, namely NE1532 (*agrA*), NE119 (*ausA*), NE188 (*mfd*), NE873 (*agrC*), NE1140

(*lysA*), and NE117 (*cydA*). Strains with transposon insertions in *agrA*, *agrC* and *ausA* showed a highly significant reduction in PI-uptake AUC (adjusted $p=5.4x10^{-4}$, Wilcoxon rank-sum test), confirming their reported roles in affecting bacterial cytotoxicity and validating our convergence analysis (Figure 5F) (Blättner et al., 2016; Das et al., 2016; Laabei et al., 2021; Mairpady Shambat et al., 2016). We extended this analysis and used high-content, high-throughput microscopy to observe and quantify in an unbiased manner the impact of each mutation on the *S. aureus* infectivity and intracellular persistence (see methods). There was an inverse relationship between *InToxSa* and high-content imaging outputs, with the three mutants most reduced in cytotoxicity showing both a higher percentage of infected cells recovered after 24 hours of infection, and a high number of bacteria per infected cell at 24h post-infection as compared to the wild type control JE2 (Figure 5G, H).

Functional assessment of specific convergent mutations

To further assess the impact of specific convergent mutations on intracellular cytotoxicity, we used site-directed mutagenesis in *S. aureus* BPH3370 (ST239) to recreate a subset of the convergent mutations. We selected isolate BPH3370 for these experiments as it displayed high *InToxSa* PI-uptake AUC (comparable to JE2, Figure 4C) cytotoxicity without bearing any of the convergent mutations we intended to introduce. We focused our attention on mutations likely to affect protein function and based on the attenuation in cytotoxicity of the cognate transposon mutants. We selected six mutations, previously not documented nor characterised, including non-synonymous mutations leading to residue substitution (*agrA* E7K and *cydA* R390C [a reversion of C390R]), frameshifts leading to truncated proteins (*agrC* G310 frameshift, *ausA* K2308 frameshift, and *lysA* K354 frameshift), and introduction of a stop codon (*mfd* W568 stop codon) in the sequences of convergent genes (Figure 6A, and Figure 6 Supplementary Figure 1). We then used *InToxSa* to assess the cytotoxicity of each targeted mutant, compared to BPH3370 wild type, JE2 and the

343

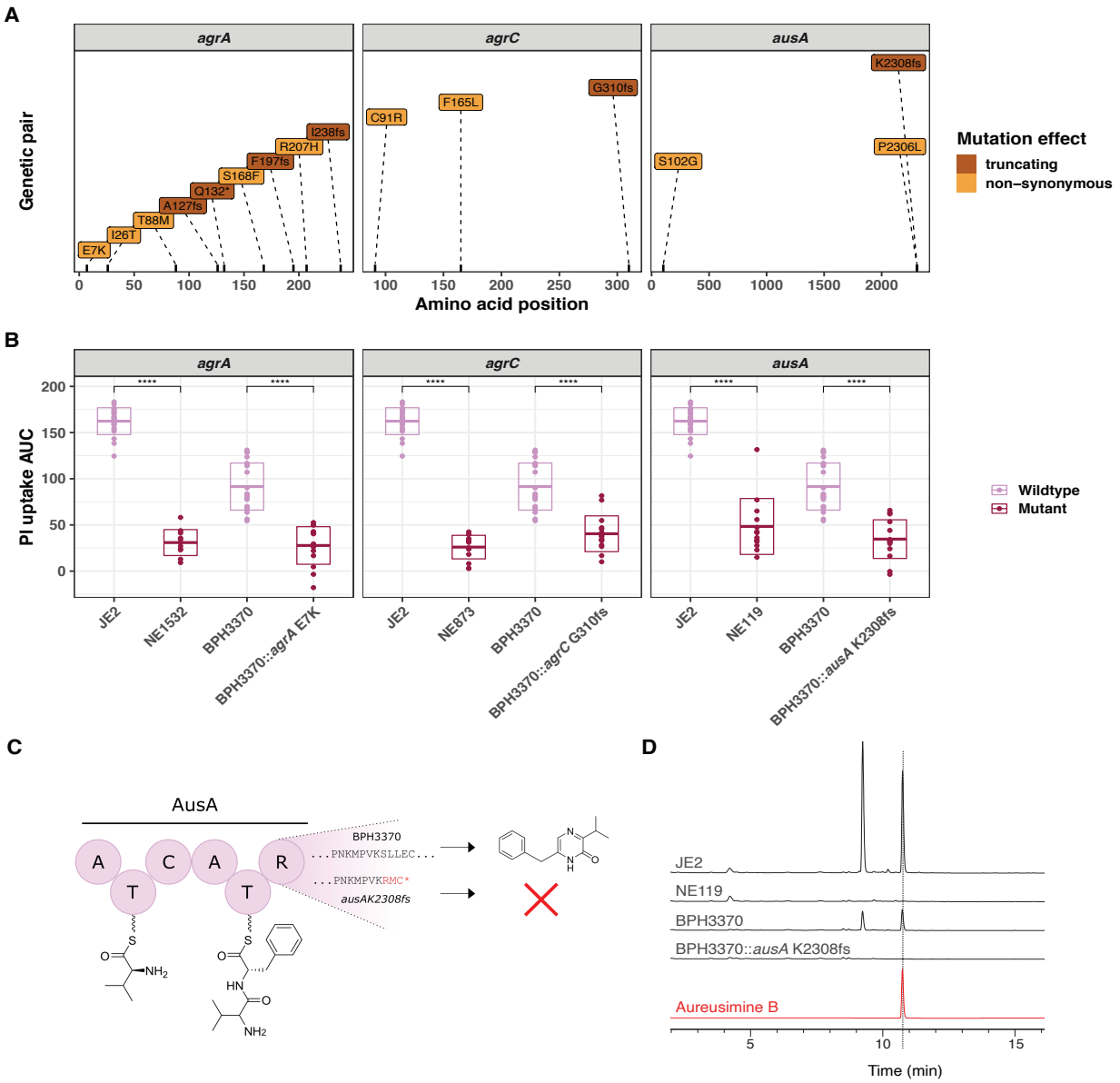

Fig 6. Introduction of convergent agrA, agrC and ausA mutations in the clinical isolate BPH3370 reduces its intracellular cytotoxicity while ausA mutation affects aureusimine B production.

(A) Position and nature of convergent mutations identified in the genes agrA, agrC and ausA. For each gene, the amino acid position affected by mutations is shown on the x-axis for each gene. Convergent mutations causing a significant contrasting PI uptake phenotype are colored according to their consequence on protein function: non-synonymous (orange), truncating (characterized by the introduction of a frameshift (fs) or a strop codon (*) (maroon). (B) Effect of convergent mutations on the intracellular cytotoxicity of the clinical isolate BPH3370. The PI uptake AUC values for JE2, the cognate Nebraska transposon mutants of convergent genes, BPH3370 wildtype and BPH3370 bearing the mutations affecting agrA, agrC, and *ausA. The crossbar represents mean and standard deviation (P<0.0001). (C) Predicted impact of K2308fs mutation on aureusimines synthesis (D) HPLC analysis of S. aureus ethyl-acetate extracts for aureusimines compared to an Aureusimine B synthetic standard.*

344 corresponding JE2 Nebraska transposon mutant, for each of the six loci (Figure 6B, Figure 6-figure
345 supplement 1). We observed that recreation of the E7K *agrA* mutation, the *agrC* G310 frameshift
346 mutation and the *ausA* K2308 frameshift mutations lead to a significant reduction in intracellular
347 cytotoxicity in BPH3370 (Figure 6B). However, the W568 stop codon *mfd* mutation, the K354
348 frameshift *lysA* mutation and the *cydA* R390C mutation had no significant effect on the cytotoxicity
349 of the BPH3370 strain (Figure 6 - Supplementary Figure 1). It is noteworthy that transposon
350 insertions in these three genes also had a less pronounced effect on the phenotype of JE2 strain as
351 compared to the *agr* and *ausA* loci (Figure 5F).
352
353 We predicted that the *ausA* K2308 frameshift causing a 11 base pair deletion mutation in BPH3370
354 would lead to a loss of aureusimine biosynthesis. This was because the frameshift occurred within
355 the *ausA* reducing domain and would thus prevent the release of the dipeptide L-Val-L-Tyr~T2 to
356 form the intermediate amino aldehyde, with no cyclization to form the imine (Figure 6C)
357 (Zimmermann & Fischbach, 2010). As expected, HPLC analysis confirmed the absence of
358 aureusimines in the BPH3370 K2308fs mutant, similarly to the transposon *ausA* mutant (NE119)
359 (Figure 6D).
360
361 **Discussion**
362 Recurrent and persistent staphylococcal infections have been proposed to result from within-host
363 selective pressures leading to the evolution of adaptive traits by the bacteria, a process also
364 observed in other human bacterial pathogens (Didelot et al., 2016; Gatt & Margalit, 2021; Giulieri,
365 Guérillot, Duchene, et al., 2022). The emergence of mutations affecting regulators controlling toxin
366 production has been proposed as a mechanism enabling *S. aureus* to adapt to its host while evading
367 cellular immune responses (Giulieri, Guérillot, Duchene, et al., 2022; Young et al., 2012, 2017).
368 Identifying the molecular signatures supporting the pathoadaptation of *S. aureus* at the host cell

interface is important for understanding how *S. aureus* can cause persistent, difficult-to-treat infections lasting many months (Gao et al., 2015).

Several studies of *S. aureus* clinical isolates have attempted to identify such signatures by assessing the cytotoxicity of bacterial supernatants applied onto host cells, in an *ex-cellulo* fashion (Giulieri et al., 2018; McConville et al., 2022; Recker et al., 2017). Such assessments would be adequate if *S. aureus* was an extracellular pathogen exerting its cytotoxicity from without host cells (Soe et al., 2021), but *S. aureus* is a facultative intracellular pathogen able to invade and persist in a wide range of eukaryotic cells (Al Kindi et al., 2019; Krauss et al., 2019; Luqman et al., 2019; Musilova et al., 2019; Sinha & Fraunholz, 2010). We developed the *InToxSa* cytotoxicity assay to address this shortcoming and to try and identify *S. aureus* pathoadaptive mutations that support a *S. aureus* intracellular lifestyle. By harnessing the power of comparative and statistical bacterial genomics with *InToxSa* readouts for a large collection of bacteraemia-associated *S. aureus* isolates, we identified mutations in *S. aureus* that reduced the intracellular cytotoxicity and increased intracellular persistence.

We showed the performance and sensitivity of *InToxSa* with the identification of cytotoxicity differences between *S. aureus* isolates that had not previously been detected by *ex-cellulo* methods (Figure 3) (Giulieri et al., 2018). The difference in phenotypic outputs for both methods may be in part explained by the different cell types exploited for the readout (THP1 macrophages for Trypan blue exclusion assay versus HeLa-229 epithelial cells for *InToxSa*) and the bacterial fraction examined (culture supernatants versus bacterial cells) (Figure 3). The capacity of *InToxSa* to detect subtle phenotypes missed by gross cytotoxicity assessments is also conferred by its temporally granular and objective measurements of PI-uptake as a marker of host cell viability. *InToxSa* assesses the *S. aureus* toxicity caused by bacterial virulence factors produced in response to the intracellular

environment and is proportional to a defined bacterial load. This approach contrasts with methods relying on the presence of toxins accumulating over time in bacterial supernatants and whose production relies almost solely on the functionality of the Agr quorum sensing system (Altman et al., 2018; Giulieri et al., 2018; McConville et al., 2022).

We further showed the performance of this analytical pipeline by readily identifying mutations in loci such as the Agr quorum sensing system, which is well known to control *S. aureus* cytolytic activity (Giulieri et al., 2018; Giulieri, Guérillot, Duchene, et al., 2022; Laabei et al., 2021; Mairpady Shambat et al., 2016; Recker et al., 2017). However, our approach also enabled discovery of mutations in less characterised systems, including changes in *ausA*, that reduced *S. aureus* cytotoxicity and increased intracellular persistence of clinical isolates. AusA is a non-ribosomal peptide synthetase responsible for production of aureusimines, pyrazinone secondary metabolites. Our observations are consistent with previous reports showing that aureusimines contribute to the phagosomal escape of *S. aureus* JE2 to the cytosol (Blättner et al., 2016; Wilson et al., 2013). Interestingly, *S. aureus* mutants that were most affected in cytotoxicity also had a propensity to persist intracellularly (Figure 5). Infected host cells have been proposed as trojan horses for intracellular *S. aureus*, increasing the risks of systemic dissemination to organs, such as the liver and kidneys, following bacteraemia and contribute to infection persistence (Jorch et al., 2019; Surewaard et al., 2016; Thwaites & Gant, 2011). Whilst *agr*-dysfunctional isolates were associated with persistent infections (Fowler, Jr. et al., 2004; Schweizer et al., 2011), intracellular persistence caused by mutations in *agr* loci could possibly constitute a population bottleneck (Pollitt et al., 2018; Spaan et al., 2013). However, such population bottlenecks may be transient as it has been suggested that mutations arising in *agr* defective pathoadapted clinical isolates could possibly compensate for the loss of *agr* functionality and restore *S. aureus* virulence, suggesting a stepwise within-host evolution of clinical isolates (Altman et al., 2018; Giulieri, Guérillot, Duchene, et al., 2022).

Current statistical genomics strategies in human genetic support combining allele-counting methods (GWAS), for the detection of common variants, with comparative genomics approaches to identify rare variants (Singh et al., 2022; Trubetskoy et al., 2022). In microbial genomics, this strategy is best achieved by combining microbial GWAS and convergent evolution studies (Chen & Shapiro, 2021; Giulieri, Guérillot, Holmes, et al., 2022; Guérillot et al., 2018; Saund & Snitkin, 2020). Whilst our GWAS approach only identified *agrA* as significantly associated with low cytotoxicity (Figure 4E), our evolutionary convergence analysis on genetic pairs among our 387 bacteraemia isolates identified mutations in several *S. aureus* genes that led to reduced cytotoxicity (Figure 5). However, only convergent mutations occurring in *agrA*, *agrC* and *ausA* were confirmed to affect the cytotoxicity and intracellular persistence phenotypes when introduced into a clinical isolate (Figure 6). This may be due to epistatic effects or combinations of mutations within a specific *S. aureus* strain may be acting in concert to control the expression of the numerous bacterial cytolytic determinants, underscoring the need to functionally confirm the findings of the convergence analysis

Our study also shows that intracellular cytotoxicity levels vary between sequence types. Despite causing bacteraemia, the ST22 and ST239 isolates were overall less cytotoxic than the ST8 isolates in our collection (as shown on the heatmap in Figure 4A), further corroborated by the direct cytotoxicity comparison between strains JE2 (ST8) and BPH3370 (ST239) (Figure 6B). The evolution of reduced Agr functionality (and thus cytotoxicity) in hospital-acquired ST239 and ST22 isolates has already been reported by our group and others and is confirmed by the *InToxSa* outputs (Baines et al., 2015; Collins et al., 2008; Giulieri et al., 2018; Laabei et al., 2021; Li et al., 2016). Consistent with their reduced cytotoxicity and with our hypothesis of inverse correlation between toxicity and intracellular replication, ST239 isolates caused higher degrees of bacterial persistence in infected animal models (Baines et al., 2015; Li et al., 2016) and showed increased intracellular persistence in

444 osteoblasts (Bongiorno et al., 2021). Within the limits of our experimental settings, the relatively
445 lower cytotoxicity of ST239 and ST22 isolates indicates that the amplitude of this phenotype should
446 probably be considered within a genetic lineage. The inclusion of representative isolates per lineage,
447 with defined cytotoxicity levels, would identify cytotoxicity thresholds and perhaps allowing
448 identification of more subtle genomic changes affecting phenotypes. Moreover, some of the loci
449 detected by the convergence and GWAS analyses may also have more pronounced effects in some
450 lineages than in others. For instance, mutations affecting tarL and SecA2 may affect the export and
451 secretion of virulence factors that are only present in a subset of lineages, thus explaining the
452 absence of effect on cytotoxicity caused by the cognate transposon mutants (Figure 5F).
453
454 We developed *InToxSa* using HeLa cells, a well-defined, adherent, and non-phagocytic cellular
455 model (Das et al., 2016; Stelzner, Hertlein, et al., 2020; Stelzner, Winkler, et al., 2020). We used
456 adherent epithelial cells because they can be maintained for extended infection periods and so
457 allow the acquisition of useful kinetic measurements of cytotoxicity. However, we also acknowledge
458 the limitation in using these cells in that they do not have the bactericidal modalities of the
459 phagocytes encountered by *S. aureus* in the bloodstream (Brinkmann, 2004; Chow et al., 2020;
460 Krause et al., 2019). Neutrophils are amongst the first immune cells to engage *S. aureus* during
461 bacteraemia (Brinkmann, 2004). However, neutrophils have a relatively short *in vitro* lifespan
462 following their purification from blood and would not be well-suited to an *InToxSa*-style assay
463 format (Ge et al., 2020; Rosales, 2020; Tak et al., 2013; Zwack et al., 2022). Polymorphonuclear cell
464 lines such as HL-60, exploited in other *ex-cellulo* assays, may represent an alternative to primary
465 neutrophils (McConville et al., 2022; Rose et al., 2015). These cells display some of the same
466 important biological functions as neutrophils, including neutrophil extracellular traps (NETs)
467 (Scieszka et al., 2020), critical in the clearing of *S. aureus* (Brinkmann, 2004; Greenlee-Wacker et al.,
468 2014; Zwack et al., 2022). While PI-uptake by these cells could be used as a readout of their viability,

HL-60 cells also don't cover all the bactericidal enzymatic activities of primary neutrophils, a potential limitation for their use (Nordenfelt et al., 2009; Yaseen et al., 2017).

We used *InToxSa* to identify *S. aureus* pathoadaptive mutations, enriched in bacterial populations that are associated with human disease (e.g., upon transit from colonising to invasive). We hypothesised that these mutations would support an intracellular persistence for *S. aureus*. Our future research will focus on understanding how these genetic changes might be allowing the bacterium to avoid cell-intrinsic surveillance systems, such as lytic programmed cell death; the self-destructive processes restricting systemic progression of intracellular bacterial pathogens (Wanford et al., 2022). Unlike well-described intracellular gram-negative bacteria, *S. aureus* does not have effector proteins to block lytic programmed cell death (Soe et al., 2021). Pathoadaptive mutations such as those arising in the *agr* locus might prevent cellular injuries caused by *S. aureus* toxins under Agr control, that would be sensed by cell-intrinsic surveillance platforms such as the inflammasomes and trigger cell death (Krause et al., 2019; Soe et al., 2021). Loss-of-function mutations in *ausA*, preventing the biosynthesis of aureusimines might be confining *S. aureus* to a lysosomal compartment where the bacteria have the potential to replicate, and conceivably evade host surveillance mechanisms (Blättner et al., 2016; Flannagan et al., 2016; Grosz et al., 2014; Moldovan & Fraunholz, 2019).

Conclusion

Current large-scale comparative genomics of *S. aureus* bacteraemia isolates can be further refined by including underexplored pathogenicity traits such as the capacity of *S. aureus* to invade and survive in host cells. We have addressed this poorly characterised trait of *S. aureus* pathogenicity by creating the *InToxSa* assay that measures the intracellular cytotoxicity of many hundreds of *S. aureus* clinical isolates at scale. We showcase the robustness and reproducibility of phenotypic

494 outputs which, in combination with comparative and statistical genomics, have confidently
495 identified convergent mutations arising in *agr* and *ausA* genes that reduced the intracellular
496 cytotoxicity and increased the intracellular persistence of bacteraemia isolates during infection. The
497 adoption of the *InToxSa* methodology in future pheno-genomics studies would improve the
498 detection of pathoadaptive mutations supporting the persistence and relapse of *S. aureus*
499 infections.

500

501 ## Materials and Methods

502 *S. aureus isolates*

503 Clinical isolates were selected from a combined collection of 843 clinical isolates of *S. aureus*
504 bacteraemia (Giulieri et al., 2018) that was obtained from the vancomycin sub-studies of the
505 Australian and New Zealand Cooperative on Outcome in Staphylococcal Sepsis (ANZCOSS) study
506 (Holmes, JID 2012) and the Vancomycin Efficacy in Staphylococcal Sepsis in Australasia (VANESSA)
507 study (Holmes, BMC Infectious Diseases 2018). We selected 387 isolates to maximise the likelihood
508 to detect phenotype-genotype associations by sampling different lineages and enriching for
509 episodes where multiple isolates per patient were available. See supplementary file 3.

510

511 *Whole genome sequencing*

512 After subculturing strains twice from -80C glycerol stock, DNA was extracted using the Janus®
513 automated workstation (PerkinElmer) or manual extraction kits (Invitrogen PureLink genomic DNA
514 kit or the Sigma GenElute kit). Normalised DNA (at a concentration of 0.2 ng/ml) was prepared for
515 sequencing using Nextera® XT DNA (Illumina) and sequencing was performed on Illumina MiSeq and
516 NextSeq platforms. Reads quality was assessed based on mean read depth and percentage of *S.*
517 *aureus* reads as computed using Kraken2 (Wood et al., 2019). Reads were assembled using Shovill,
518 an assembly pipeline that optimises the Spades assembler (https://github.com/tseemann/shovill).

519 Annotation was performed using Prokka, with a minimal contig size of 500 bp (Seemann, 2014).
520 Assembly and annotation metrics were used to further quality control of the reads. Genetic distance
521 between clinical isolates was calculated using Mash with a sketch size of 10,000 (Ondov et al., 2016).
522 We used the distance matrix generated by Mash to perform multidimensional scaling (MDS) using
523 the function 'cmdscale()' in base R. Multi-locus sequence type (ST) were inferred from the
524 assemblies using mlst (https://github.com/tseemann/mlst). We assessed the correlation between
525 the most prevalent ST and the MDS axes using the get_correlations() function in the R package
526 bugwas (Earle et al., 2016).
527
528 *Variants calling: single reference*
529 Clinical isolates' reads were mapped to internal reference BPH2947 (accession GCF_900620245.1),
530 a sequence type 239 reference genome that was generated from the collection. We used snippy,
531 v4.6.0 for mapping and variant calling, with default settings (https://github.com/tseemann/snippy).
532 The core genome alignment was constructed using Snippy-core. We defined core genome as
533 positions where at least 90% of the sequences had a minimum coverage of 10 reads and used
534 Goalign v0.3.4 and SNP-sites v2.5.1 to extract core genome positions. To infer a maximum likelihood
535 phylogenetic tree of the clinical isolates collection we ran IQ-TREE v2.0.3 using a GTR-G4 model. We
536 used HomoplasyFinder (Crispell, Microb Genomics 2019) to identify homoplasic sites based on the
537 consistency index. The consistency index was calculated with the following formula: (Number of
538 nucleotides at site -1)/Minimum number of changes on tree.
539
540 *Construction of mutants by allelic exchange.*
541 Engineering of convergent mutations in *agrA*, *agrC*, *ausA, mfd*, *lysA,* and *cydA* genes in the strain
542 BPH3370 was performed by allelic exchange as described previously (Monk & Stinear, 2021) using
543 oligonucleotides described in supplementary table 7 (outlining residues modified by convergent

544 mutations). Upstream and downstream regions of each mutation were PCR amplified and gel
545 extracted and then a splice by overlap extension (SOE) PCR was performed to generate each insert.
546 Each insert was cloned into linearised pIMAY-Z vector by Seamless Ligation Cloning Extract (SLiCE)
547 cloning (Zhang et al., 2012) to generate six plasmids. Each plasmid was separately transformed into
548 *E. coli* strain IM08B (Monk et al., 2015) confirmed by colony PCR, then purified and transformed into
549 *S. aureus* strain BPH3370 by electroporation. Mutant candidates were screened by Sanger
550 Sequencing (Australian Genome Research Facility, Melbourne, VIC, AUS) and positive clones were
551 validated by whole genome sequencing (WGS) on an Illumina Miseq or NextSeq550 platforms
552 (Illumina, San Diego, CA, USA) to confirm their genotype. The resultant reads were mapped to the
553 BPH3370 reference genome and mutations were identified using snippy (v4.6.0,
554 https://github.com/tseemann/snippy).
555
556 *Clinical isolates library preparation*
557 The collection of clinical isolates was prepared to be readily inoculated from 96-well microtiter
558 plates. Clinical isolates were grown in 10 ml Brain Heart Infusion (BHI) broth (BD Bacto) from single
559 colonies to stationary phase. Briefly, a volume corresponding to 1-unit OD600 for each culture was
560 centrifuged at 10,000 x g for 5 min. The bacterial pellets were washed once with 500 µL of fresh BHI
561 and centrifuged again. The washed bacterial pellets were resuspended in 600 µL of storage media
562 (BHI containing 40% glycerol), vortexed briefly and 200 µL were distributed across 96-well microtiter
563 plates. To prevent operator and plate effect biases, the 387 isolates were randomly distributed with
564 each plate to include 29 distinct isolates, represented in non-contiguous technical triplicates. Built-
565 in controls for cytotoxicity were included in each plate. The wild-type JE2 strain was used as positive
566 cytotoxicity control and the BPH3757 strain, an ST239 isolate bearing the T88M *agrA* mutation
567 described in (Giulieri et al., 2018), as a non-cytotoxic control. Six wells were kept empty to monitor

568 the viability of non-infected controls and account for residual PI uptake. Plates were stored at -80°C.
569 Each plate was at least tested in 3 biological replicates.
570
571 *Tissue culture*
572 HeLa-CCL2 cells (ATCC) were maintained and propagated in Dubelcco's Modified Eagle Medium
573 (DMEM) + GlutaMAX (4.5 g/L D-Glucose and 110 mg/L sodium pyruvate) supplemented with heat-
574 inactivated 10% Foetal Bovine Serum (Gibco) and in absence of antibiotics.
575
576 *InToxSa assay*
577 *S. aureus* isolates were inoculated directly from stabbed frozen parsed plates stock into 100 µL of
578 BHI broth dispatched in flat bottom 96-well microtiter plates. Inoculated plates were incubated for
579 16 hours in a heat-controlled plate reader (CLARIOstar plate reader, BMG Labtech) set at 37°C.
580 Bacterial growth was assessed by OD^{600} measurement every 10 min. The endpoint optical densities
581 of cultures were used to infer bacterial density (1-unit OD^{600} corresponding to $5*10^8$ bacteria/ml).
582 Bacterial cultures were standardised and serially diluted in DMEM to reach a multiplicity of infection
583 (MOI)~10. 100 µL of bacterial suspension were added to infect 40,000 HeLa-CCL2 cells grown (70%
584 confluence per well) in 96 well black plates, clear bottom (Sigma). Infection was synchronised by
585 centrifugation at 500 x g for 10 min (Eppendorf 5810R) at room temperature. Infected plates were
586 incubated 2h at 37°C and 5% CO2 to allow for *S. aureus* internalization. The infective media was
587 then discarded, and cells washed once with sterile PBS and further incubated 1h with 100 µL DMEM
588 containing cell impermeable antibiotics (80 µg/ml gentamicin (Baxter) and 10 µg/ml of lysostaphin
589 (Ambi)) at 37°C and 5% CO2 (Kim et al., 2019). This first step of antibiotic-protection assay was
590 followed by another using a lower antibiotic concentration (40 µg/ml gentamicin and 10 µg/ml
591 lysostaphin), in media supplemented with 5% FBS (Gibco), and 1 µg/ml propidium iodide, a live cell-
592 impermeant nucleic acid dye (Sigma). Plates were then incubated in the CLARIOstar Plus plate

reader (BMG Labtech) set at 37°C and 5% CO2 throughout the infection (up to 20 h post-infection). The fluorescence signal emitted by PI positive cells was acquired every 6 min from each well (excitation at 535 nm, emission at 617 nm, using the spiral well scanning mode with 50 flashes per well). Non-infected control cells were permeabilised with 0.1% Triton X-100 to determine the maximum level PI uptake and HeLa cell death.

High-content imaging

The Operetta high content microscope (PerkinElmer) was employed to accurately quantify and analyse intracellular persistence at the single-cell resolution. HeLa-CCL2 cells were seeded in Cell Carrier-96 black and optically clear bottom plates (PerkinElmer) to reach a density of 15,000 cells per well at the day of infection. HeLa cells were infected as described in the above section. Post-infection, cells were washed twice with sterile PBS and fixed with 40µl of freshly prepared 4% paraformaldehyde (PFA, ThermoFisher Scientific) for 10 minutes. Fixed cells were further washed five times and stored at 4°C in PBS. Fixed cells were first permeabilised with 40µl of 0.2% Triton X-100 for 3 minutes, washed thrice with PBS, and incubated one hour in 40µl of blocking solution (PBS-BSA 3%). Bacteria were detected with polyclonal antibodies raised in rabbits against whole fixed cells of *S. aureus* USA300 strains, JE2::*spa*, BPH2919 and BPH3672 (WEHI antibody technology platform, https://www.wehi.edu.au/research/research-technologies/antibody-technologies). Sera were used at 1:1000, diluted in PBS-BSA 3%, tween 0.05% for 5 hours at room temperature. Wells were then washed thrice with PBS and incubated 45 min with a secondary antibody (donkey anti-rabbit coupled to Alexa 488, 1:2000 dilution, Invitrogen) in PBS-BSA 3% containing 0.05% Tween-20 (Sigma) and 10% normal donkey serum (Abcam). Wells were washed thrice with PBS and incubated with Phalloidin-TRITC (1:4000) and DAPI (1:4000) (Sigma) in PBS for 15 min. Finally, wells were washed 5 times with PBS and covered with 200µl of PBS. Plates were covered with aluminium foil and stored at 4°C until image acquisition on the Operetta microscope.

Confocal microscopy

HeLa-CCL2 grown on coverslips were infected using the same conditions described above. Coverslips were treated with PBS supplemented with 1% BSA and 0.2% triton-X100 for 20 minutes at room temperature to permeabilize cells and incubated overnight in a blocking buffer (PBS supplemented with 1% BSA and 0.1% Tween 20). Coverslips were then probed one hour at room temperature with an anti-LAMP1 monoclonal antibody (1:250, clone H4A3 (mouse), Developmental Studies Hybridoma Bank) and 1:1000 polyclonal anti-*S. aureus* diluted in blocking buffer supplemented with 10% normal goat serum (Abcam). Coverslips were washed thrice with then incubated overnight at 4°C with 1:2000 anti-rabbit (488), anti-mouse (647) secondary antibodies diluted in blocking buffer supplemented with 10% normal goat serum. Coverslips were then incubated 7 minutes with DAPI (1:5000), washed 5 times and mounted in Prolong Gold antifade (ThermoFisher Scientific). Samples were imaged on the Zeiss LSM780 confocal microscope.

High-content imaging acquisition and analysis

Cells were analyzed using the Operetta CLS high-content analysis system (Perkin Elmer). For each well, images were acquired in a single plane at 11 non-overlapping fields of view (675 x 508µm / 1360x1024 pixels in size) using a 20x PLAN long working distance objective (NA 0.45). DAPI fluorescence (HeLa cell nuclei) was imaged with the filter set: excitation = 360–400nm, emission: 410–480nm; 50ms exposure). A488 fluorescence (*S. aureus*) was imaged with the filter set: excitation = 460-490nm, emission = 500-550nm; exposure = 200ms. A594 fluorescence (HeLa actin stained by Phalloidin-TRITC) was imaged with the filter set "StdOrange1/Cy3" filter set (excitation: 520–550nm, emission: 560–630nm; 0.5-sec exposure).

Image processing and analysis were performed using the PhenoLOGIC™ machine learning option in the Harmony software (Perkin Elmer, v4.1). Nuclei were segmented from the DAPI channel using

643 the 'Find Nuclei algorithm' (Method B, Area filter > 40µm^2, Common Threshold of 0.4). Cells were
644 segmented from the A594 channels using the Find Cells algorithm (Method C, Area filter > 100µm^2,
645 Common Threshold of 0.5). The A488 signals corresponding to *S. aureus* were further processed
646 using a sliding parabola (curvature, 50 pixels) and Gaussian filter (filter width, 1 pixel) to remove
647 noise and improve the signal-to-noise ratio. *S. aureus* were segmented by applying the Find Spots
648 algorithm (Method A, Relative Spot Intensity 0.280, Splitting Co-efficient 0.5).
649
650 *Processing of PI fluorescence signals*
651 For every 96 well plate, the PI uptake data for each well at each timepoint were standardised to the
652 JE2 strain control using Proportion Of Maximum Scoring (POMS): (PI uptake – min(Pi uptake [JE2]))
653 / range(PI uptake [JE2]). Experiments with less than two JE2 replicates available per plate were
654 excluded from our analyses. Standardized data were used to fit a cubic smoothing spline (Little,
655 2013) using the R function smooth.spline(). Technical replicates within each plate were classified as
656 outliers and excluded if > 10% of their timepoint values differed by more than 1.5 times the
657 interquartile range (Tukey method), between the fitted value and the mean for a given isolate. After
658 excluding outlier replicates, fitted data were used to calculate the following PI uptake parameters:
659 area under the curve (AUC), maximum PI uptake rate (rmax), peak PI uptake (µmax), time to
660 maximum PI uptake rate (t(rmax)), time to peak PI uptake (t(µ max)), trough PI uptake, time of
661 trough, and final PI uptake.
662
663 *Dimensionality reduction of PI uptake data*
664 Principal component analysis was performed using the 'dudi.pca()` function in the R package
665 `adegenet` and the randomForest package in R was used for fitting an unsupervised random Forest
666 model. We used the similarity matrix generated by the model to define similarity cluster of PI
667 uptake. We used the output of the random forest model to calculate the importance of each PI

668 uptake parameter defined as mean decrease in Gini index and mean decrease in accuracy (Breiman,
669 2001).
670
671 *PI uptake GWAS*
672 We transformed the mean PI-uptake AUC data using the automated normalisation package
673 bestNormalize in R. A genome-wide association study (GWAS) using the normalised AUC data and
674 the 158,169 core genome variants (all positions where at least 90% of the strains had at least 10
675 reads coverage, see above) obtained after mapping isolates reads to reference genome BPH2947.
676 To correct for the population structure, we used the factored spectrally transformed linear mixed
677 models (FaST-LMM) implemented in *pyseer* v1.3.6 (Lees et al., 2018). Random effects in Fast-LMM
678 were computed from a kinship matrix based on the core genome SNPs generated by Gemma v0.98.1
679 (Zhou and Stephens, 2012). The Bonferroni method was used to correct P values for multiple testing.
680 We performed the GWAS using single variants and the gene-burden test implemented in pyseer.
681 We excluded synonymous mutations for single variants and gene-burden GWAS. As suggested in
682 the pyseer documentation (https://pyseer.readthedocs.io/en/master/index.html), we kept only
683 mutations with a minimum allele fraction (MAF) of 0.01 and at least two independent acquisitions
684 across the phylogeny in the single variants GWAS and only rare mutations (MAF < 0.01) in the gene-
685 burden GWAS. For consistent annotation of mutations, we identified BPH2947 genes homologs
686 using BLASTP and annotated FPR3757 genes using *aureowiki* (Fuchs et al., 2018) and *Microbesonline*
687 (Alm et al., 2005). The GWAS analysis was run using a customised in-house pipeline
688 (https://github.com/stefanogg/CLOGEN).
689
690 *Determination of genetic pairs with contrasting PI uptake*
691 Isolate pairs for the convergent evolution analysis were identified by screening pairs separated by
692 less than 200 mutations distance for statistically significant differences in the PI uptake AUC (Mann-

693 Whitney test), wherein an isolate causing low PI uptake (isolate 2) was compared to a reference
694 isolate causing higher PI uptake (isolate 1). The genetic distance between closely related isolates
695 was calculated using Snippy and is based on the number of variants identified when mapping the
696 reads of isolate 2 on the draft assembly of isolate 1 (Higgs et al., 2022). To avoid biases related to
697 assembly errors and uneven reads coverage between the two isolates, variants calls were filtered
698 as previously described (https://github.com/stefanogg/staph_adaptation_paper) (Giulieri,
699 Guérillot, Duchene, et al., 2022). Non-redundant and phylogenetically independent genetic pairs
700 were identified by manual inspection of the phylogenetic tree.
701
702 *Genetic pairs analysis*
703 Mutations identified in genetic pairs and filtered as described above were further characterised
704 using a multilayered annotation strategy as previously described (Giulieri, Guérillot, Duchene, et al.,
705 2022). Firstly, mutated coding regions (amino-acid sequences) across draft genomes were clustered
706 using CD-HIT. We then used BLASTP to identify homologs of each cluster within the *S. aureus*
707 USA300 FPR3757 reference genome that was annotated using the AureoWiki repository (Fuchs et
708 al., 2018), with a 90% identity and 50% coverage threshold. As genetic pairs were phylogenetically
709 independent and non-redundant, emergence of the same mutation or mutations in the same locus
710 in multiple pairs indicated convergent evolution and was suggestive of positive selection. Based on
711 this, we ranked USA300 FPR3757 homologs according to the number of pairs with mutations.
712
713 *Code and data availability*

714 Scripts to process PI uptake data and to perform genomic analyses are available on github at
715 https://github.com/stefanogg/*InToxSa*. The code for genomic analyses is available on
716 https://github.com/stefanogg/CLOGEN (GWAS analysis),

717 and on https://github.com/stefanogg/staph_adaptation_paper (comparative genomics of genetic
718 pairs).

719

720 Whole genome sequences of the 387 clinical strains are available in the European Nucleotide
721 Archive under Bioproject accession number PRJEB27932.

722

723 *Aureusimine B identification*

724 Bacterial extracts were isolated from 30 ml cultures grown in TSB at 37°C overnight under agitation.
725 Bacterial cells were pelleted by centrifugation at 4000 x g during 30 min and the culture
726 supernatants were sterilized by passage through a 0.22mM filter. For each strain, 10 millilitres of
727 supernatant were added to an equal volume of ethyl acetate in glass tubes, vortexed and allowed
728 to extract at room temperature overnight. Ethyl acetate extracts were dried *in vacuo*. Dried ethyl
729 acetate extracts were resuspended in 100 ml methanol and 2ml of each sample was analyzed by
730 HPLC using the Shimadzu Prominence HPLC system coupled to a SPD-M20A diode array detector.
731 The column oven (CTO-20A) was set to 40°C and aureusimine B was separated on Kinetex C18, 75 x
732 3mm, 2.6 µm column (Phenomenex). Purified aureusimine B was used as reference standard
733 (Bioaustralis Fine Chemicals). All used chemicals were of analytical grade.
734 Samples were run with water, 0.1% TFA (solvent A) and acetonitrile (solvent B). The gradient elution
735 was performed on the HPLC at a flow rate of 0.5ml/min as follows: 10% B for 3.5 mins, 10-100% B
736 over 12.5 mins, 100-10% B over 1 min, then 10% B for 7 mins (total run time, 24 mins).

737

738 **References**

739

740 Al Kindi, A., Alkahtani, A. M., Nalubega, M., El-Chami, C., O'Neill, C., Arkwright, P. D., & Pennock, J.
741 L. (2019). Staphylococcus aureus Internalized by Skin Keratinocytes Evade Antibiotic Killing.
742 *Frontiers in Microbiology*, *10*, 2242. https://doi.org/10.3389/fmicb.2019.02242

743 Alm, E. J., Huang, K. H., Price, M. N., Koche, R. P., Keller, K., Dubchak, I. L., & Arkin, A. P. (2005). The
744 MicrobesOnline Web site for comparative genomics. *Genome Research*, *15*(7), 1015–1022.
745 https://doi.org/10.1101/gr.3844805

746 Altman, D. R., Sullivan, M. J., Chacko, K. I., Balasubramanian, D., Pak, T. R., Sause, W. E., Kumar, K.,
747 Sebra, R., Deikus, G., Attie, O., Rose, H., Lewis, M., Fulmer, Y., Bashir, A., Kasarskis, A.,
748 Schadt, E. E., Richardson, A. R., Torres, V. J., Shopsin, B., & van Bakel, H. (2018). Genome
749 Plasticity of *agr* -Defective Staphylococcus aureus during Clinical Infection. *Infection and*
750 *Immunity*, *86*(10), e00331-18. https://doi.org/10.1128/IAI.00331-18

751 Baines, S. L., Holt, K. E., Schultz, M. B., Seemann, T., Howden, B. O., Jensen, S. O., van Hal, S. J.,
752 Coombs, G. W., Firth, N., Powell, D. R., Stinear, T. P., & Howden, B. P. (2015). Convergent
753 Adaptation in the Dominant Global Hospital Clone ST239 of Methicillin-Resistant
754 Staphylococcus aureus. *MBio*, *6*(2), e00080-15. https://doi.org/10.1128/mBio.00080-15

755 Blättner, S., Das, S., Paprotka, K., Eilers, U., Krischke, M., Kretschmer, D., Remmele, C. W., Dittrich,
756 M., Müller, T., Schuelein-Voelk, C., Hertlein, T., Mueller, M. J., Huettel, B., Reinhardt, R.,
757 Ohlsen, K., Rudel, T., & Fraunholz, M. J. (2016). Staphylococcus aureus Exploits a Non-
758 ribosomal Cyclic Dipeptide to Modulate Survival within Epithelial Cells and Phagocytes.
759 *PLOS Pathogens*, *12*(9), e1005857. https://doi.org/10.1371/journal.ppat.1005857

760 Bongiorno, D., Musso, N., Caruso, G., Lazzaro, L. M., Caraci, F., Stefani, S., & Campanile, F. (2021).
761 *Staphylococcus aureus* ST228 and ST239 as models for expression studies of diverse
762 markers during osteoblast infection and persistence. *MicrobiologyOpen*, *10*(2).
763 https://doi.org/10.1002/mbo3.1178

764 Breiman, L. (2001). [No title found]. *Machine Learning*, *45*(1), 5–32.
765 https://doi.org/10.1023/A:1010933404324
766 Brinkmann, V. (2004). Neutrophil Extracellular Traps Kill Bacteria. *Science*, *303*(5663), 1532–1535.
767 https://doi.org/10.1126/science.1092385
768 Chen, P. E., & Shapiro, B. J. (2021). *Classic genome-wide association methods are unlikely to*
769 *identify causal variants in strongly clonal microbial populations* [Preprint]. Genomics.
770 https://doi.org/10.1101/2021.06.30.450606
771 Cheung, G. Y. C., Bae, J. S., & Otto, M. (2021). Pathogenicity and virulence of Staphylococcus
772 aureus. *Virulence*, *12*(1), 547–569. https://doi.org/10.1080/21505594.2021.1878688
773 Chow, S. H., Deo, P., Yeung, A. T. Y., Kostoulias, X. P., Jeon, Y., Gao, M.-L., Seidi, A., Olivier, F. A. B.,
774 Sridhar, S., Nethercott, C., Cameron, D., Robertson, A. A. B., Robert, R., Mackay, C. R.,
775 Traven, A., Jin, Z.-B., Hale, C., Dougan, G., Peleg, A. Y., & Naderer, T. (2020). Targeting
776 NLRP3 and staphylococcal pore-forming toxin receptors in human-induced pluripotent
777 stem cell-derived macrophages. *Journal of Leukocyte Biology*.
778 https://doi.org/10.1002/JLB.4MA0420-497R
779 Collins, J., Buckling, A., & Massey, R. C. (2008). Identification of factors contributing to T-cell
780 toxicity of Staphylococcus aureus clinical isolates. *Journal of Clinical Microbiology*, *46*(6),
781 2112–2114. https://doi.org/10.1128/JCM.00156-08
782 Dankoff, J. G., Pallister, K. B., Guerra, F. E., Parks, A. J., Gorham, K., Mastandrea, S., Voyich, J. M., &
783 Nygaard, T. K. (2020). Quantifying the Cytotoxicity of Staphylococcus aureus Against
784 Human Polymorphonuclear Leukocytes. *Journal of Visualized Experiments*, *155*, 60681.
785 https://doi.org/10.3791/60681
786 Das, S., Lindemann, C., Young, B. C., Muller, J., Österreich, B., Ternette, N., Winkler, A.-C.,
787 Paprotka, K., Reinhardt, R., Förstner, K. U., Allen, E., Flaxman, A., Yamaguchi, Y., Rollier, C.
788 S., van Diemen, P., Blättner, S., Remmele, C. W., Selle, M., Dittrich, M., … Fraunholz, M. J.

(2016). Natural mutations in a *Staphylococcus aureus* virulence regulator attenuate cytotoxicity but permit bacteremia and abscess formation. *Proceedings of the National Academy of Sciences*, *113*(22), E3101–E3110. https://doi.org/10.1073/pnas.1520255113

Didelot, X., Walker, A. S., Peto, T. E., Crook, D. W., & Wilson, D. J. (2016). Within-host evolution of bacterial pathogens. *Nature Reviews Microbiology*, *14*(3), 150–162. https://doi.org/10.1038/nrmicro.2015.13

Earle, S. G., Wu, C.-H., Charlesworth, J., Stoesser, N., Gordon, N. C., Walker, T. M., Spencer, C. C. A., Iqbal, Z., Clifton, D. A., Hopkins, K. L., Woodford, N., Smith, E. G., Ismail, N., Llewelyn, M. J., Peto, T. E., Crook, D. W., McVean, G., Walker, A. S., & Wilson, D. J. (2016). Identifying lineage effects when controlling for population structure improves power in bacterial association studies. *Nature Microbiology*, *1*(5), 16041. https://doi.org/10.1038/nmicrobiol.2016.41

Fey, P. D., Endres, J. L., Yajjala, V. K., Widhelm, T. J., Boissy, R. J., Bose, J. L., & Bayles, K. W. (2013). A Genetic Resource for Rapid and Comprehensive Phenotype Screening of Nonessential Staphylococcus aureus Genes. *MBio*, *4*(1), e00537-12. https://doi.org/10.1128/mBio.00537-12

Flannagan, R. S., Heit, B., & Heinrichs, D. E. (2016). Intracellular replication of Staphylococcus aureus in mature phagolysosomes in macrophages precedes host cell death, and bacterial escape and dissemination. *Cellular Microbiology*, *18*(4), 514–535. https://doi.org/10.1111/cmi.12527

Flannagan, R. S., Kuiack, R. C., McGavin, M. J., & Heinrichs, D. E. (2018). Staphylococcus aureus Uses the GraXRS Regulatory System To Sense and Adapt to the Acidified Phagolysosome in Macrophages. *MBio*, *9*(4). https://doi.org/10.1128/mBio.01143-18

812 Foster, T. J., Geoghegan, J. A., Ganesh, V. K., & Höök, M. (2014). Adhesion, invasion and evasion:
813 The many functions of the surface proteins of Staphylococcus aureus. *Nature Reviews*
814 *Microbiology*, *12*(1), 49–62. https://doi.org/10.1038/nrmicro3161
815 Fowler, Jr., V. G., Sakoulas, G., McIntyre, L. M., Meka, V. G., Arbeit, R. D., Cabell, C. H., Stryjewski,
816 M. E., Eliopoulos, G. M., Reller, L. B., Corey, G. R., Jones, T., Lucindo, N., Yeaman, M. R., &
817 Bayer, A. S. (2004). Persistent Bacteremia Due to Methicillin-Resistant *Staphylococcus*
818 *aureus* Infection Is Associated with *agr* Dysfunction and Low-Level In Vitro Resistance to
819 Thrombin-Induced Platelet Microbicidal Protein. *The Journal of Infectious Diseases*, *190*(6),
820 1140–1149. https://doi.org/10.1086/423145
821 Fuchs, S., Mehlan, H., Bernhardt, J., Hennig, A., Michalik, S., Surmann, K., Pané-Farré, J., Giese, A.,
822 Weiss, S., Backert, L., Herbig, A., Nieselt, K., Hecker, M., Völker, U., & Mäder, U. (2018a).
823 Aureo Wiki-The repository of the Staphylococcus aureus research and annotation
824 community. *International Journal of Medical Microbiology*, *308*(6), 558–568.
825 https://doi.org/10.1016/j.ijmm.2017.11.011
826 Gao, W., Monk, I. R., Tobias, N. J., Gladman, S. L., Seemann, T., Stinear, T. P., & Howden, B. P.
827 (2015). Large tandem chromosome expansions facilitate niche adaptation during persistent
828 infection with drug-resistant Staphylococcus aureus. *Microbial Genomics*, *1*(2).
829 https://doi.org/10.1099/mgen.0.000026
830 Gatt, Y. E., & Margalit, H. (2021). Common Adaptive Strategies Underlie Within-Host Evolution of
831 Bacterial Pathogens. *Molecular Biology and Evolution*, *38*(3), 1101–1121.
832 https://doi.org/10.1093/molbev/msaa278
833 Ge, C., Monk, I. R., Monard, S. C., Bedford, J. G., Braverman, J., Stinear, T. P., & Wakim, L. M.
834 (2020). Neutrophils play an ongoing role in preventing bacterial pneumonia by blocking the
835 dissemination of *Staphylococcus aureus* from the upper to the lower airways. *Immunology*
836 *& Cell Biology*, *98*(7), 577–594. https://doi.org/10.1111/imcb.12343

837 Giulieri, S. G., Baines, S. L., Guerillot, R., Seemann, T., Gonçalves da Silva, A., Schultz, M., Massey,
838 R. C., Holmes, N. E., Stinear, T. P., & Howden, B. P. (2018). Genomic exploration of
839 sequential clinical isolates reveals a distinctive molecular signature of persistent
840 Staphylococcus aureus bacteraemia. *Genome Medicine*, *10*(1), 65.
841 https://doi.org/10.1186/s13073-018-0574-x
842 Giulieri, S. G., Guérillot, R., Duchene, S., Hachani, A., Daniel, D., Seemann, T., Davis, J. S., Tong, S.
843 Y., Young, B. C., Wilson, D. J., Stinear, T. P., & Howden, B. P. (2022). Niche-specific genome
844 degradation and convergent evolution shaping Staphylococcus aureus adaptation during
845 severe infections. *ELife*, *11*, e77195. https://doi.org/10.7554/eLife.77195
846 Giulieri, S. G., Guérillot, R., Holmes, N. E., Baines, S. L., Hachani, A., Daniel, D. S., Seemann, T.,
847 Davis, J. S., Van Hal, S., Tong, S. Y. C., Stinear, T. P., & Howden, B. P. (2022). *A statistical*
848 *genomics framework to trace bacterial genomic predictors of clinical outcomes in*
849 Staphylococcus aureus *bacteraemia* [Preprint]. Infectious Diseases (except HIV/AIDS).
850 https://doi.org/10.1101/2022.04.21.22273941
851 Greenlee-Wacker, M. C., Rigby, K. M., Kobayashi, S. D., Porter, A. R., DeLeo, F. R., & Nauseef, W.
852 M. (2014). Phagocytosis of *Staphylococcus aureus* by Human Neutrophils Prevents
853 Macrophage Efferocytosis and Induces Programmed Necrosis. *The Journal of Immunology*,
854 *192*(10), 4709–4717. https://doi.org/10.4049/jimmunol.1302692
855 Grosz, M., Kolter, J., Paprotka, K., Winkler, A.-C., Schäfer, D., Chatterjee, S. S., Geiger, T., Wolz, C.,
856 Ohlsen, K., Otto, M., Rudel, T., Sinha, B., & Fraunholz, M. (2014). Cytoplasmic replication of
857 Staphylococcus aureus upon phagosomal escape triggered by phenol-soluble modulin α.
858 *Cellular Microbiology*, *16*(4), 451–465. https://doi.org/10.1111/cmi.12233
859 Guérillot, R., Gonçalves da Silva, A., Monk, I., Giulieri, S., Tomita, T., Alison, E., Porter, J., Pidot, S.,
860 Gao, W., Peleg, A. Y., Seemann, T., Stinear, T. P., & Howden, B. P. (2018). Convergent
861 Evolution Driven by Rifampin Exacerbates the Global Burden of Drug-Resistant

Staphylococcus aureus. *MSphere*, *3*(1), e00550-17. https://doi.org/10.1128/mSphere.00550-17

Higgs, C., Sherry, N. L., Seemann, T., Horan, K., Walpola, H., Kinsella, P., Bond, K., Williamson, D. A., Marshall, C., Kwong, J. C., Grayson, M. L., Stinear, T. P., Gorrie, C. L., & Howden, B. P. (2022). Optimising genomic approaches for identifying vancomycin-resistant Enterococcus faecium transmission in healthcare settings. *Nature Communications*, *13*(1), 509. https://doi.org/10.1038/s41467-022-28156-4

Holmes, N. E., Turnidge, J. D., Munckhof, W. J., Robinson, J. O., Korman, T. M., O'Sullivan, M. V. N., Anderson, T. L., Roberts, S. A., Gao, W., Christiansen, K. J., Coombs, G. W., Johnson, P. D. R., & Howden, B. P. (2011). Antibiotic Choice May Not Explain Poorer Outcomes in Patients With Staphylococcus aureus Bacteremia and High Vancomycin Minimum Inhibitory Concentrations. *The Journal of Infectious Diseases*, *204*(3), 340–347. https://doi.org/10.1093/infdis/jir270

Holmes, N. E., Turnidge, J. D., Munckhof, W. J., Robinson, J. O., Korman, T. M., O'Sullivan, M. V. N., Anderson, T. L., Roberts, S. A., Warren, S. J. C., Coombs, G. W., Tan, H.-L., Gao, W., Johnson, P. D. R., & Howden, B. P. (2014). Genetic and molecular predictors of high vancomycin MIC in Staphylococcus aureus bacteremia isolates. *Journal of Clinical Microbiology*, *52*(9), 3384–3393. https://doi.org/10.1128/JCM.01320-14

Jorch, S. K., Surewaard, B. G., Hossain, M., Peiseler, M., Deppermann, C., Deng, J., Bogoslowski, A., van der Wal, F., Omri, A., Hickey, M. J., & Kubes, P. (2019). Peritoneal GATA6+ macrophages function as a portal for Staphylococcus aureus dissemination. *The Journal of Clinical Investigation*, *129*(11), 4643–4656. https://doi.org/10.1172/JCI127286

Kim, J.-H., Chaurasia, A. K., Batool, N., Ko, K. S., & Kim, K. K. (2019). Alternative Enzyme Protection Assay To Overcome the Drawbacks of the Gentamicin Protection Assay for Measuring Entry

and Intracellular Survival of Staphylococci. *Infection and Immunity*, *87*(5), e00119-19. https://doi.org/10.1128/IAI.00119-19

Krause, K., Daily, K., Estfanous, S., Hamilton, K., Badr, A., Abu Khweek, A., Hegazi, R., Anne, M. N., Klamer, B., Zhang, X., Gavrilin, M. A., Pancholi, V., & Amer, A. O. (2019). Caspase-11 counteracts mitochondrial ROS-mediated clearance of *Staphylococcus aureus* in macrophages. *EMBO Reports*, *20*(12). https://doi.org/10.15252/embr.201948109

Krauss, J. L., Roper, P. M., Ballard, A., Shih, C.-C., Fitzpatrick, J. A. J., Cassat, J. E., Ng, P. Y., Pavlos, N. J., & Veis, D. J. (2019). Staphylococcus aureus Infects Osteoclasts and Replicates Intracellularly. *MBio*, *10*(5), e02447-19. https://doi.org/10.1128/mBio.02447-19

Laabei, M., Peacock, S. J., Blane, B., Baines, S. L., Howden, B. P., Stinear, T. P., & Massey, R. C. (2021). Significant variability exists in the cytotoxicity of global methicillin-resistant Staphylococcus aureus lineages. *Microbiology*, *167*(12). https://doi.org/10.1099/mic.0.001119

Laabei, M., Recker, M., Rudkin, J. K., Aldeljawi, M., Gulay, Z., Sloan, T. J., Williams, P., Endres, J. L., Bayles, K. W., Fey, P. D., Yajjala, V. K., Widhelm, T., Hawkins, E., Lewis, K., Parfett, S., Scowen, L., Peacock, S. J., Holden, M., Wilson, D., … Massey, R. C. (2014). Predicting the virulence of MRSA from its genome sequence. *Genome Research*, *24*(5), 839–849. https://doi.org/10.1101/gr.165415.113

Laabei, M., Uhlemann, A.-C., Lowy, F. D., Austin, E. D., Yokoyama, M., Ouadi, K., Feil, E., Thorpe, H. A., Williams, B., Perkins, M., Peacock, S. J., Clarke, S. R., Dordel, J., Holden, M., Votintseva, A. A., Bowden, R., Crook, D. W., Young, B. C., Wilson, D. J., … Massey, R. C. (2015). Evolutionary Trade-Offs Underlie the Multi-faceted Virulence of Staphylococcus aureus. *PLOS Biology*, *13*(9), e1002229. https://doi.org/10.1371/journal.pbio.1002229

Lâm, T.-T., Giese, B., Chikkaballi, D., Kühn, A., Wolber, W., Pané-Farré, J., Schäfer, D., Engelmann, S., Fraunholz, M., & Sinha, B. (2010). Phagolysosomal Integrity Is Generally Maintained

911 after *Staphylococcus aureus* Invasion of Nonprofessional Phagocytes but Is Modulated by
912 Strain 6850. *Infection and Immunity*, *78*(8), 3392–3403. https://doi.org/10.1128/IAI.00012-
913 10

914 Lees, J. A., Galardini, M., Bentley, S. D., Weiser, J. N., & Corander, J. (2018). pyseer: A
915 comprehensive tool for microbial pangenome-wide association studies. *Bioinformatics*,
916 *34*(24), 4310–4312. https://doi.org/10.1093/bioinformatics/bty539

917 Li, M., Dai, Y., Zhu, Y., Fu, C.-L., Tan, V. Y., Wang, Y., Wang, X., Hong, X., Liu, Q., Li, T., Qin, J., Ma, X.,
918 Fang, J., & Otto, M. (2016). Virulence determinants associated with the Asian community-
919 associated methicillin-resistant Staphylococcus aureus lineage ST59. *Scientific Reports*,
920 *6*(1), 27899. https://doi.org/10.1038/srep27899

921 Little, T. D. (2013). *Longitudinal structural equation modeling*. The Guilford Press.

922 Luqman, A., Ebner, P., Reichert, S., Sass, P., Kabagema-Bilan, C., Heilmann, C., Ruth, P., & Götz, F.
923 (2019). A new host cell internalisation pathway for SadA-expressing staphylococci triggered
924 by excreted neurochemicals. *Cellular Microbiology*, *21*(9).
925 https://doi.org/10.1111/cmi.13044

926 Mairpady Shambat, S., Siemens, N., Monk, I. R., Mohan, D. B., Mukundan, S., Krishnan, K. C.,
927 Prabhakara, S., Snäll, J., Kearns, A., Vandenesch, F., Svensson, M., Kotb, M., Gopal, B.,
928 Arakere, G., & Norrby-Teglund, A. (2016). A point mutation in AgrC determines cytotoxic or
929 colonizing properties associated with phenotypic variants of ST22 MRSA strains. *Scientific*
930 *Reports*, *6*(1), 31360. https://doi.org/10.1038/srep31360

931 Mantero, A., & Ishwaran, H. (2021). Unsupervised random forests. *Statistical Analysis and Data*
932 *Mining*, *14*(2), 144–167. https://doi.org/10.1002/sam.11498

933 McConville, T. H., Austin, E. D., Geng, W., Shi, Q., Balasubramanian, D., Kubin, C. J., Torres, V. J., &
934 Uhlemann, A.-C. (2022). *In Vitro* Cytotoxicity and Clinical Correlates of MRSA Bacteremia.

Antimicrobial Agents and Chemotherapy, *66*(1), e01559-21. https://doi.org/10.1128/AAC.01559-21

Moldovan, A., & Fraunholz, M. J. (2019). In or out: Phagosomal escape of Staphylococcus aureus. *Cellular Microbiology*, *21*(3), e12997. https://doi.org/10.1111/cmi.12997

Monk, I. R., & Stinear, T. P. (2021). From cloning to mutant in 5 days: Rapid allelic exchange in Staphylococcus aureus. *Access Microbiology*, *3*(2). https://doi.org/10.1099/acmi.0.000193

Monk, I. R., Tree, J. J., Howden, B. P., Stinear, T. P., & Foster, T. J. (2015). Complete Bypass of Restriction Systems for Major Staphylococcus aureus Lineages. *MBio*, *6*(3), e00308-15. https://doi.org/10.1128/mBio.00308-15

Murray, C. J., Ikuta, K. S., Sharara, F., Swetschinski, L., Robles Aguilar, G., Gray, A., Han, C., Bisignano, C., Rao, P., Wool, E., Johnson, S. C., Browne, A. J., Chipeta, M. G., Fell, F., Hackett, S., Haines-Woodhouse, G., Kashef Hamadani, B. H., Kumaran, E. A. P., McManigal, B., … Naghavi, M. (2022). Global burden of bacterial antimicrobial resistance in 2019: A systematic analysis. *The Lancet*, *399*(10325), 629–655. https://doi.org/10.1016/S0140-6736(21)02724-0

Musilova, J., Mulcahy, M. E., Kuijk, M. M., McLoughlin, R. M., & Bowie, A. G. (2019). Toll-like receptor 2-dependent endosomal signaling by Staphylococcus aureus in monocytes induces type I interferon and promotes intracellular survival. *The Journal of Biological Chemistry*, *294*(45), 17031–17042. https://doi.org/10.1074/jbc.RA119.009302

Nordenfelt, P., Bauer, S., Lönnbro, P., & Tapper, H. (2009). Phagocytosis of Streptococcus pyogenes by All-Trans Retinoic Acid-Differentiated HL-60 Cells: Roles of Azurophilic Granules and NADPH Oxidase. *PLoS ONE*, *4*(10), e7363. https://doi.org/10.1371/journal.pone.0007363

Ondov, B. D., Treangen, T. J., Melsted, P., Mallonee, A. B., Bergman, N. H., Koren, S., & Phillippy, A. M. (2016). Mash: Fast genome and metagenome distance estimation using MinHash. *Genome Biology*, *17*(1), 132. https://doi.org/10.1186/s13059-016-0997-x

Peyrusson, F., Varet, H., Nguyen, T. K., Legendre, R., Sismeiro, O., Coppée, J.-Y., Wolz, C., Tenson, T., & Van Bambeke, F. (2020). Intracellular Staphylococcus aureus persisters upon antibiotic exposure. *Nature Communications*, *11*(1), 2200. https://doi.org/10.1038/s41467-020-15966-7

Pollitt, E. J. G., Szkuta, P. T., Burns, N., & Foster, S. J. (2018). Staphylococcus aureus infection dynamics. *PLOS Pathogens*, *14*(6), e1007112. https://doi.org/10.1371/journal.ppat.1007112

Recker, M., Laabei, M., Toleman, M. S., Reuter, S., Saunderson, R. B., Blane, B., Török, M. E., Ouadi, K., Stevens, E., Yokoyama, M., Steventon, J., Thompson, L., Milne, G., Bayliss, S., Bacon, L., Peacock, S. J., & Massey, R. C. (2017). Clonal differences in Staphylococcus aureus bacteraemia-associated mortality. *Nature Microbiology*, *2*(10), 1381–1388. https://doi.org/10.1038/s41564-017-0001-x

Rosales, C. (2020). Neutrophils at the crossroads of innate and adaptive immunity. *Journal of Leukocyte Biology*, *108*(1), 377–396. https://doi.org/10.1002/JLB.4MIR0220-574RR

Rose, H. R., Holzman, R. S., Altman, D. R., Smyth, D. S., Wasserman, G. A., Kafer, J. M., Wible, M., Mendes, R. E., Torres, V. J., & Shopsin, B. (2015). Cytotoxic Virulence Predicts Mortality in Nosocomial Pneumonia Due to Methicillin-Resistant *Staphylococcus aureus*. *Journal of Infectious Diseases*, *211*(12), 1862–1874. https://doi.org/10.1093/infdis/jiu554

Saund, K., & Snitkin, E. S. (2020). Hogwash: Three methods for genome-wide association studies in bacteria. *Microbial Genomics*, *6*(11). https://doi.org/10.1099/mgen.0.000469

Schweizer, M. L., Furuno, J. P., Sakoulas, G., Johnson, J. K., Harris, A. D., Shardell, M. D., McGregor, J. C., Thom, K. A., & Perencevich, E. N. (2011). Increased Mortality with Accessory Gene

983 Regulator (*agr*) Dysfunction in *Staphylococcus aureus* among Bacteremic Patients.
984 *Antimicrobial Agents and Chemotherapy*, *55*(3), 1082–1087.
985 https://doi.org/10.1128/AAC.00918-10
986 Scieszka, D., Lin, Y.-H., Li, W., Choudhury, S., Yu, Y., & Freire, M. (2020). *Netome: The Molecular*
987 *Characterization of Neutrophil Extracellular Traps (NETs)* [Preprint]. Immunology.
988 https://doi.org/10.1101/2020.05.18.102772
989 Seemann, T. (2014). Prokka: Rapid prokaryotic genome annotation. *Bioinformatics*, *30*(14), 2068–
990 2069. https://doi.org/10.1093/bioinformatics/btu153
991 Siboo, I. R., Chambers, H. F., & Sullam, P. M. (2005). Role of SraP, a Serine-Rich Surface Protein of
992 *Staphylococcus aureus* , in Binding to Human Platelets. *Infection and Immunity*, *73*(4),
993 2273–2280. https://doi.org/10.1128/IAI.73.4.2273-2280.2005
994 Siegmund, A., Afzal, M. A., Tetzlaff, F., Keinhörster, D., Gratani, F., Paprotka, K., Westermann, M.,
995 Nietzsche, S., Wolz, C., Fraunholz, M., A. Hübner, C., Löffler, B., & Tuchscherr, L. (2021).
996 Intracellular persistence of *Staphylococcus aureus* in endothelial cells is promoted by the
997 absence of phenol-soluble modulins. *Virulence*, *12*(1), 1186–1198.
998 https://doi.org/10.1080/21505594.2021.1910455
999 Singh, T., Poterba, T., Curtis, D., Akil, H., Al Eissa, M., Barchas, J. D., Bass, N., Bigdeli, T. B., Breen,
1000 G., Bromet, E. J., Buckley, P. F., Bunney, W. E., Bybjerg-Grauholm, J., Byerley, W. F.,
1001 Chapman, S. B., Chen, W. J., Churchhouse, C., Craddock, N., Cusick, C. M., … Daly, M. J.
1002 (2022). Rare coding variants in ten genes confer substantial risk for schizophrenia. *Nature*,
1003 *604*(7906), 509–516. https://doi.org/10.1038/s41586-022-04556-w
1004 Sinha, B., & Fraunholz, M. (2010). Staphylococcus aureus host cell invasion and post-invasion
1005 events. *International Journal of Medical Microbiology*, *300*(2–3), 170–175.
1006 https://doi.org/10.1016/j.ijmm.2009.08.019

Soe, Y. M., Bedoui, S., Stinear, T. P., & Hachani, A. (2021). Intracellular *STAPHYLOCOCCUS AUREUS* and host cell death pathways. *Cellular Microbiology*, *23*(5). https://doi.org/10.1111/cmi.13317

Spaan, A. N., Surewaard, B. G. J., Nijland, R., & van Strijp, J. A. G. (2013). Neutrophils Versus *Staphylococcus aureus*: A Biological Tug of War. *Annual Review of Microbiology*, *67*(1), 629–650. https://doi.org/10.1146/annurev-micro-092412-155746

Stelzner, K., Boyny, A., Hertlein, T., Sroka, A., Moldovan, A., Paprotka, K., Kessie, D., Mehling, H., Potempa, J., Ohlsen, K., Fraunholz, M. J., & Rudel, T. (2021). Intracellular Staphylococcus aureus employs the cysteine protease staphopain A to induce host cell death in epithelial cells. *PLOS Pathogens*, *17*(9), e1009874. https://doi.org/10.1371/journal.ppat.1009874

Stelzner, K., Hertlein, T., Sroka, A., Moldovan, A., Paprotka, K., Kessie, D., Mehling, H., Potempa, J., Ohlsen, K., Fraunholz, M. J., & Rudel, T. (2020). *Intracellular* Staphylococcus aureus *employs the cysteine protease staphopain A to induce host cell death in epithelial cells* [Preprint]. Microbiology. https://doi.org/10.1101/2020.02.10.936575

Stelzner, K., Winkler, A.-C., Liang, C., Boyny, A., Ade, C. P., Dandekar, T., Fraunholz, M. J., & Rudel, T. (2020). Intracellular Staphylococcus aureus Perturbs the Host Cell Ca^{2+} Homeostasis To Promote Cell Death. *MBio*, *11*(6), e02250-20. https://doi.org/10.1128/mBio.02250-20

Strobel, M., Pförtner, H., Tuchscherr, L., Völker, U., Schmidt, F., Kramko, N., Schnittler, H.-J., Fraunholz, M. J., Löffler, B., Peters, G., & Niemann, S. (2016). Post-invasion events after infection with Staphylococcus aureus are strongly dependent on both the host cell type and the infecting S. aureus strain. *Clinical Microbiology and Infection*, *22*(9), 799–809. https://doi.org/10.1016/j.cmi.2016.06.020

Su, M., Davis, M. H., Peterson, J., Solis-Lemus, C., Satola, S. W., & Read, T. D. (2021). Effect of genetic background on the evolution of Vancomycin-Intermediate *Staphylococcus aureus* (VISA). *PeerJ*, *9*, e11764. https://doi.org/10.7717/peerj.11764

Surewaard, B. G. J., Deniset, J. F., Zemp, F. J., Amrein, M., Otto, M., Conly, J., Omri, A., Yates, R. M., & Kubes, P. (2016). Identification and treatment of the Staphylococcus aureus reservoir in vivo. *Journal of Experimental Medicine*, *213*(7), 1141–1151. https://doi.org/10.1084/jem.20160334

Tak, T., Tesselaar, K., Pillay, J., Borghans, J. A. M., & Koenderman, L. (2013). What's your age again? Determination of human neutrophil half-lives revisited. *Journal of Leukocyte Biology*, *94*(4), 595–601. https://doi.org/10.1189/jlb.1112571

Tam, K., & Torres, V. J. (2019). Staphylococcus aureus Secreted Toxins and Extracellular Enzymes. *Microbiology Spectrum*, *7*(2). https://doi.org/10.1128/microbiolspec.GPP3-0039-2018

Thammavongsa, V., Kim, H. K., Missiakas, D., & Schneewind, O. (2015). Staphylococcal manipulation of host immune responses. *Nature Reviews Microbiology*, *13*(9), 529–543. https://doi.org/10.1038/nrmicro3521

Thwaites, G. E., & Gant, V. (2011). Are bloodstream leukocytes Trojan Horses for the metastasis of Staphylococcus aureus? *Nature Reviews Microbiology*, *9*(3), 215–222. https://doi.org/10.1038/nrmicro2508

Tong, S. Y. C., Davis, J. S., Eichenberger, E., Holland, T. L., & Fowler, V. G. (2015). Staphylococcus aureus Infections: Epidemiology, Pathophysiology, Clinical Manifestations, and Management. *Clinical Microbiology Reviews*, *28*(3), 603–661. https://doi.org/10.1128/CMR.00134-14

Trubetskoy, V., Pardiñas, A. F., Qi, T., Panagiotaropoulou, G., Awasthi, S., Bigdeli, T. B., Bryois, J., Chen, C.-Y., Dennison, C. A., Hall, L. S., Lam, M., Watanabe, K., Frei, O., Ge, T., Harwood, J. C., Koopmans, F., Magnusson, S., Richards, A. L., Sidorenko, J., … van Os, J. (2022). Mapping genomic loci implicates genes and synaptic biology in schizophrenia. *Nature*, *604*(7906), 502–508. https://doi.org/10.1038/s41586-022-04434-5

VANESSA study group, on behalf of the Australasian Society for Infectious Diseases (ASID) Clinical Research Network (CRN), Holmes, N. E., Robinson, J. O., van Hal, S. J., Munckhof, W. J., Athan, E., Korman, T. M., Cheng, A. C., Turnidge, J. D., Johnson, P. D. R., & Howden, B. P. (2018). Morbidity from in-hospital complications is greater than treatment failure in patients with Staphylococcus aureus bacteraemia. *BMC Infectious Diseases*, *18*(1), 107. https://doi.org/10.1186/s12879-018-3011-2

Wanford, J. J., Hachani, A., & Odendall, C. (2022). Reprogramming of Cell Death Pathways by Bacterial Effectors as a Widespread Virulence Strategy. *Infection and Immunity*, e0061421. https://doi.org/10.1128/iai.00614-21

Wilson, D. J., Shi, C., Teitelbaum, A. M., Gulick, A. M., & Aldrich, C. C. (2013). Characterization of AusA: A Dimodular Nonribosomal Peptide Synthetase Responsible for the Production of Aureusimine Pyrazinones. *Biochemistry*, *52*(5), 926–937. https://doi.org/10.1021/bi301330q

Wood, D. E., Lu, J., & Langmead, B. (2019). Improved metagenomic analysis with Kraken 2. *Genome Biology*, *20*(1), 257. https://doi.org/10.1186/s13059-019-1891-0

Yang, Y.-H., Jiang, Y.-L., Zhang, J., Wang, L., Bai, X.-H., Zhang, S.-J., Ren, Y.-M., Li, N., Zhang, Y.-H., Zhang, Z., Gong, Q., Mei, Y., Xue, T., Zhang, J.-R., Chen, Y., & Zhou, C.-Z. (2014). Structural Insights into SraP-Mediated Staphylococcus aureus Adhesion to Host Cells. *PLoS Pathogens*, *10*(6), e1004169. https://doi.org/10.1371/journal.ppat.1004169

Yaseen, R., Blodkamp, S., Lüthje, P., Reuner, F., Völlger, L., Naim, H. Y., & von Köckritz-Blickwede, M. (2017). Antimicrobial activity of HL-60 cells compared to primary blood-derived neutrophils against Staphylococcus aureus. *Journal of Negative Results in BioMedicine*, *16*(1), 2. https://doi.org/10.1186/s12952-017-0067-2

Yokoyama, M., Stevens, E., Laabei, M., Bacon, L., Heesom, K., Bayliss, S., Ooi, N., O'Neill, A. J., Murray, E., Williams, P., Lubben, A., Reeksting, S., Meric, G., Pascoe, B., Sheppard, S. K.,

Recker, M., Hurst, L. D., & Massey, R. C. (2018). Epistasis analysis uncovers hidden antibiotic resistance-associated fitness costs hampering the evolution of MRSA. *Genome Biology*, *19*(1), 94. https://doi.org/10.1186/s13059-018-1469-2

Young, B. C., Golubchik, T., Batty, E. M., Fung, R., Larner-Svensson, H., Votintseva, A. A., Miller, R. R., Godwin, H., Knox, K., Everitt, R. G., Iqbal, Z., Rimmer, A. J., Cule, M., Ip, C. L. C., Didelot, X., Harding, R. M., Donnelly, P., Peto, T. E., Crook, D. W., … Wilson, D. J. (2012). Evolutionary dynamics of Staphylococcus aureus during progression from carriage to disease. *Proceedings of the National Academy of Sciences*, *109*(12), 4550–4555. https://doi.org/10.1073/pnas.1113219109

Young, B. C., Wu, C.-H., Gordon, N. C., Cole, K., Price, J. R., Liu, E., Sheppard, A. E., Perera, S., Charlesworth, J., Golubchik, T., Iqbal, Z., Bowden, R., Massey, R. C., Paul, J., Crook, D. W., Peto, T. E., Walker, A. S., Llewelyn, M. J., Wyllie, D. H., & Wilson, D. J. (2017). Severe infections emerge from commensal bacteria by adaptive evolution. *ELife*, *6*, e30637. https://doi.org/10.7554/eLife.30637

Zhang, Y., Werling, U., & Edelmann, W. (2012). SLiCE: A novel bacterial cell extract-based DNA cloning method. *Nucleic Acids Research*, *40*(8), e55. https://doi.org/10.1093/nar/gkr1288

Zhou, X., & Stephens, M. (2012). Genome-wide efficient mixed-model analysis for association studies. *Nature Genetics*, *44*(7), 821–824. https://doi.org/10.1038/ng.2310

Zimmermann, M., & Fischbach, M. A. (2010). A Family of Pyrazinone Natural Products from a Conserved Nonribosomal Peptide Synthetase in Staphylococcus aureus. *Chemistry & Biology*, *17*(9), 925–930. https://doi.org/10.1016/j.chembiol.2010.08.006

Zwack, E. E., Chen, Z., Devlin, J. C., Li, Z., Zheng, X., Weinstock, A., Lacey, K. A., Fisher, E. A., Fenyö, D., Ruggles, K. V., Loke, P., & Torres, V. J. (2022). Staphylococcus aureus induces a muted host response in human blood that blunts the recruitment of neutrophils. *Proceedings of*

the National Academy of Sciences of the United States of America, *119*(31), e2123017119.

https://doi.org/10.1073/pnas.2123017119

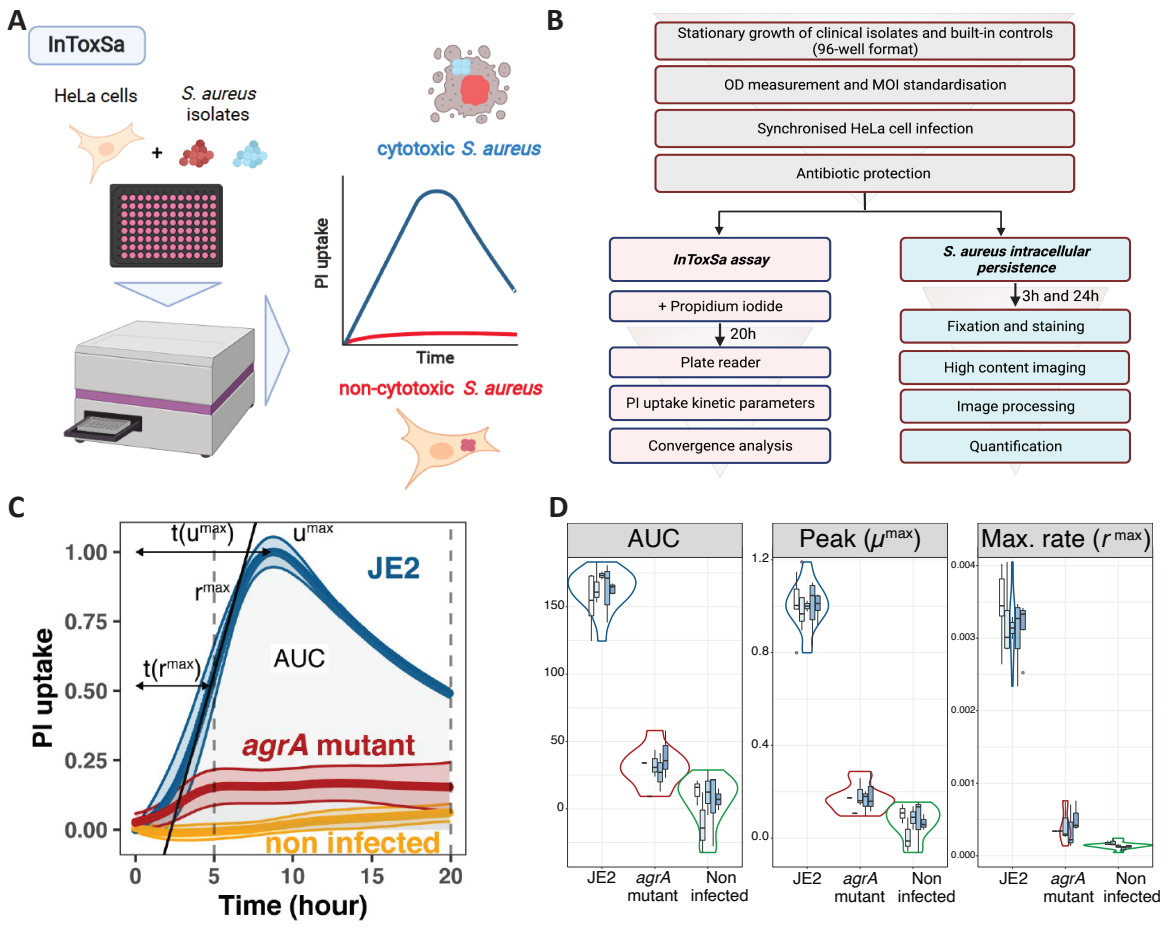
A
InToxSa
HeLa cells
S. aureus isolates
cytotoxic S. aureus
PI uptake
Time
non-cytotoxic S. aureus
B
Stationary growth of clinical isolates and built-in controls (96-well format)
OD measurement and MOI standardisation
Synchronised HeLa cell infection
Antibiotic protection
InToxSa assay
+ Propidium iodide
20h
Plate reader
PI uptake kinetic parameters
Convergence analysis
S. aureus intracellular persistence
3h and 24h
Fixation and staining
High content imaging
Image processing
Quantification
C
PI uptake
Time (hour)
t(u^max)
u^max
r^max
t(r^max)
AUC
JE2
agrA mutant
non infected
D
AUC
Peak (μ^max)
Max. rate (r^max)
JE2
agrA mutant
Non infected

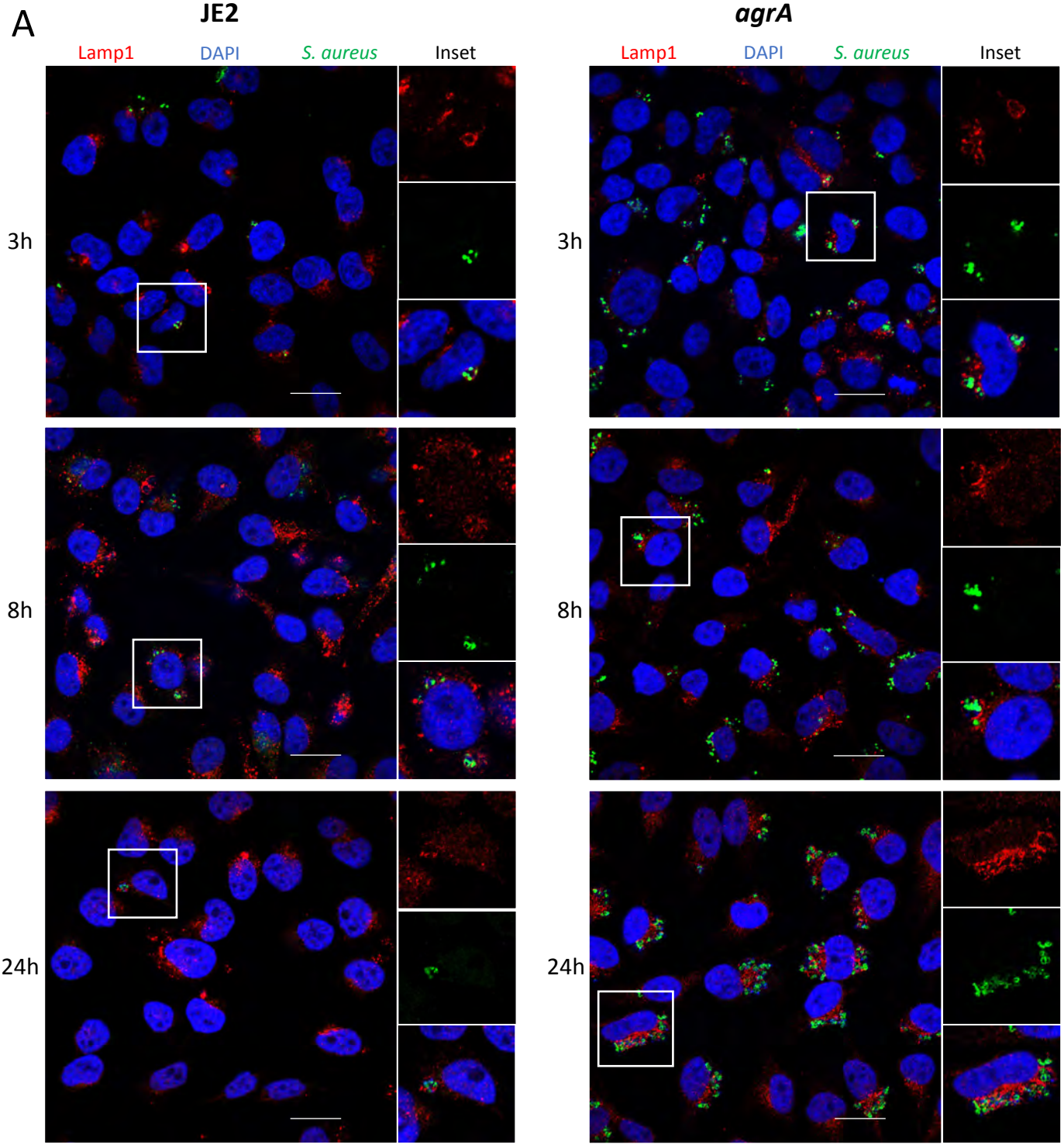
A
JE2
agrA
Lamp1
DAPI
S. aureus
Inset
3h
8h
24h

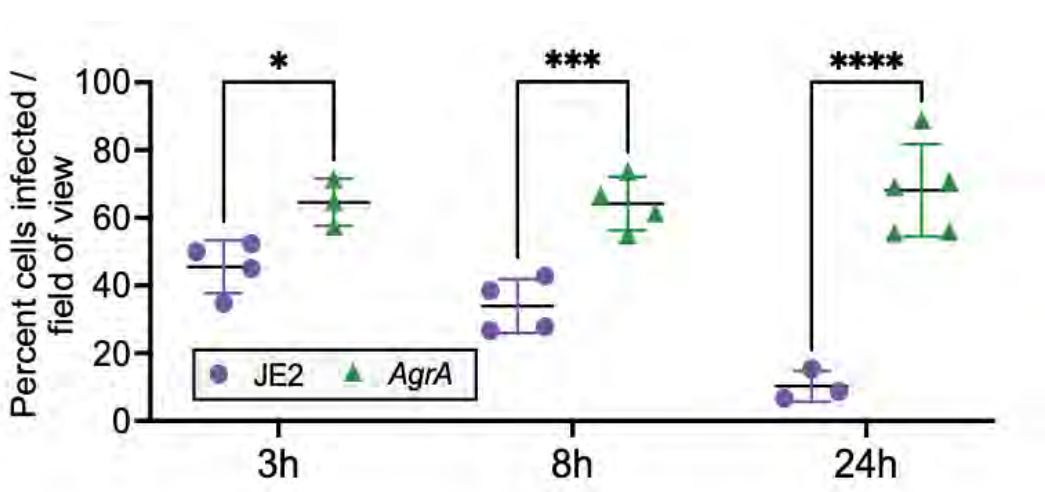
B
Percent cells infected / field of view
100
80
60
40
20
0
*
***
****
JE2
AgrA
3h
8h
24h

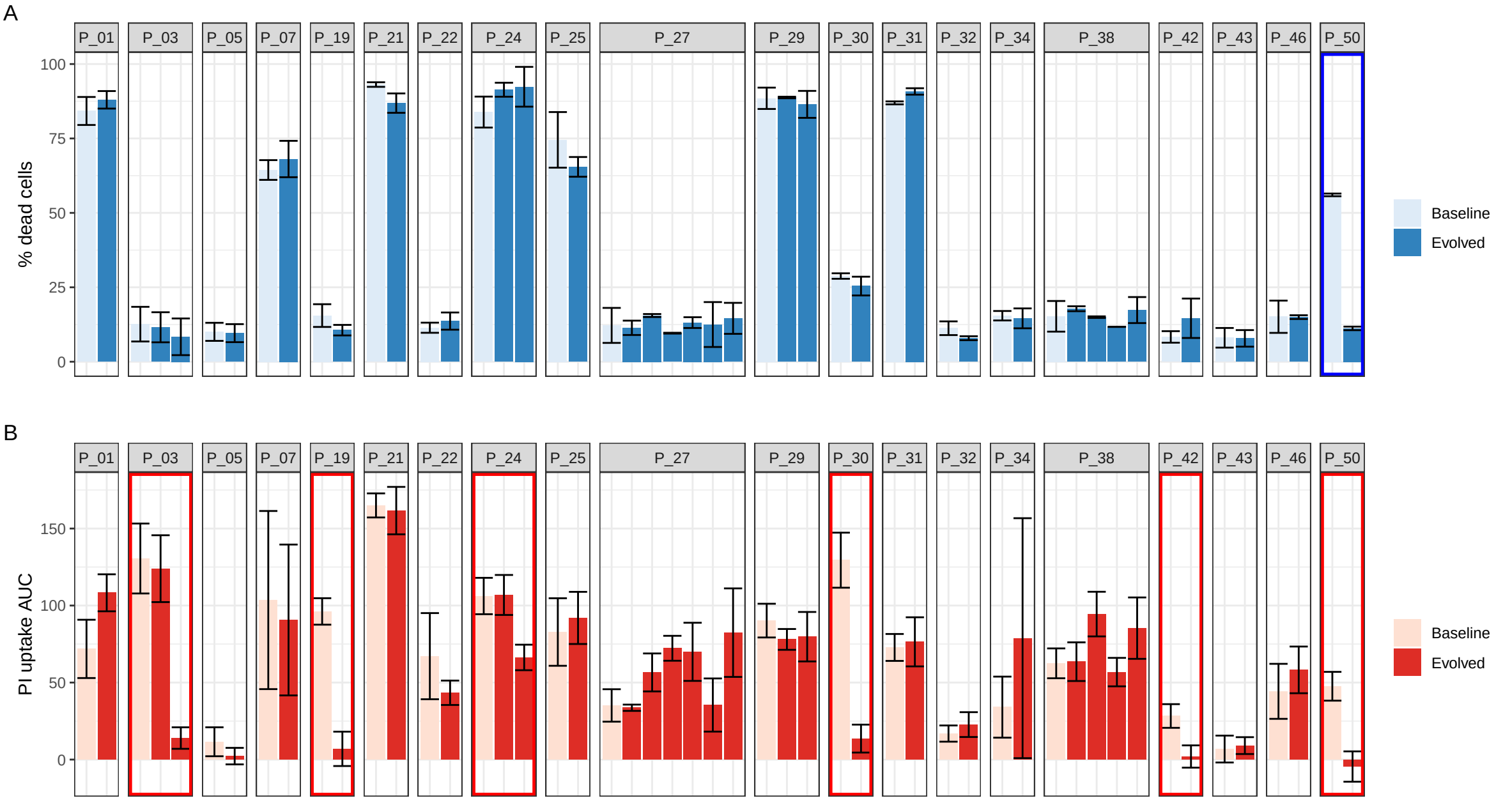
A
P_01
P_03
P_05
P_07
P_19
P_21
P_22
P_24
P_25
P_27
P_29
P_30
P_31
P_32
P_34
P_38
P_42
P_43
P_46
P_50
% dead cells
100
75
50
25
0
Baseline
Evolved
B
PI uptake AUC
150
100
50
0
Baseline
Evolved

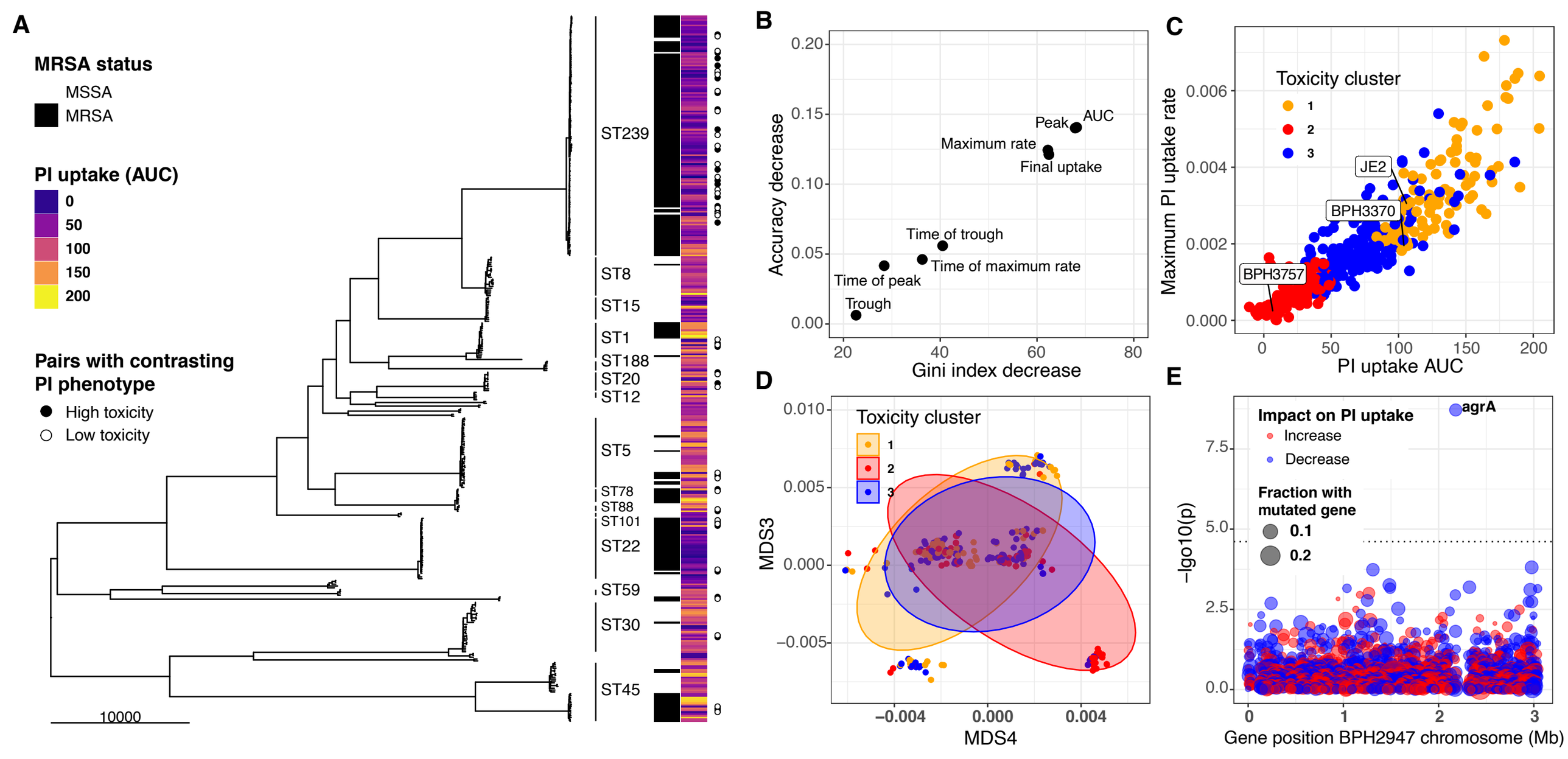
A
MRSA status
MSSA
MRSA
PI uptake (AUC)
0
50
100
150
200
Pairs with contrasting PI phenotype
High toxicity
Low toxicity
10000
ST239
ST8
ST15
ST1
ST188
ST20
ST12
ST5
ST78
ST88
ST101
ST22
ST59
ST30
ST45
B
Accuracy decrease
Gini index decrease
Peak
AUC
Maximum rate
Final uptake
Time of trough
Time of maximum rate
Time of peak
Trough
C
Toxicity cluster
1
2
3
JE2
BPH3370
BPH3757
Maximum PI uptake rate
PI uptake AUC
D
Toxicity cluster
MDS3
MDS4
E
Impact on PI uptake
Increase
Decrease
agrA
Fraction with mutated gene
0.1
0.2
−lgo10(p)
Gene position BPH2947 chromosome (Mb)

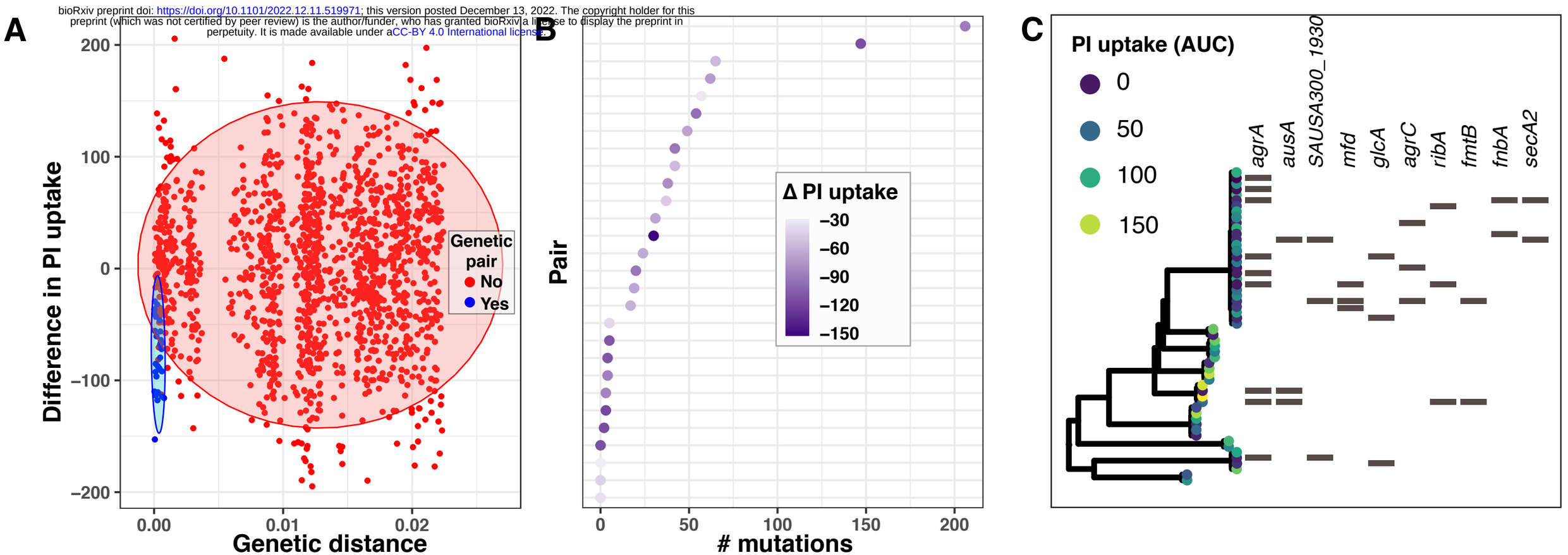

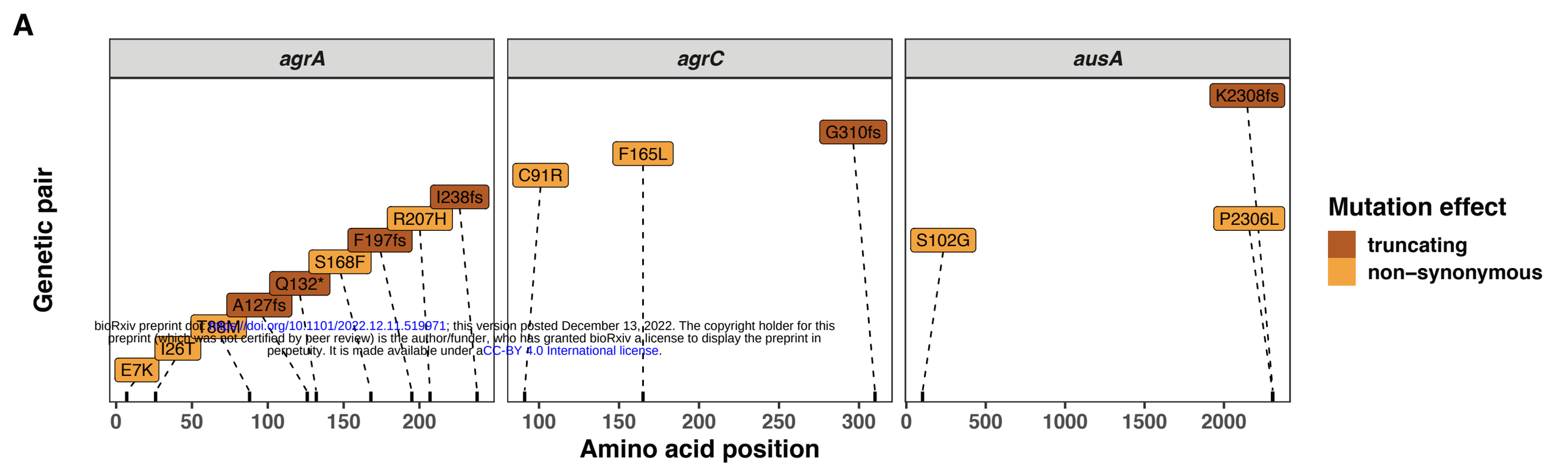

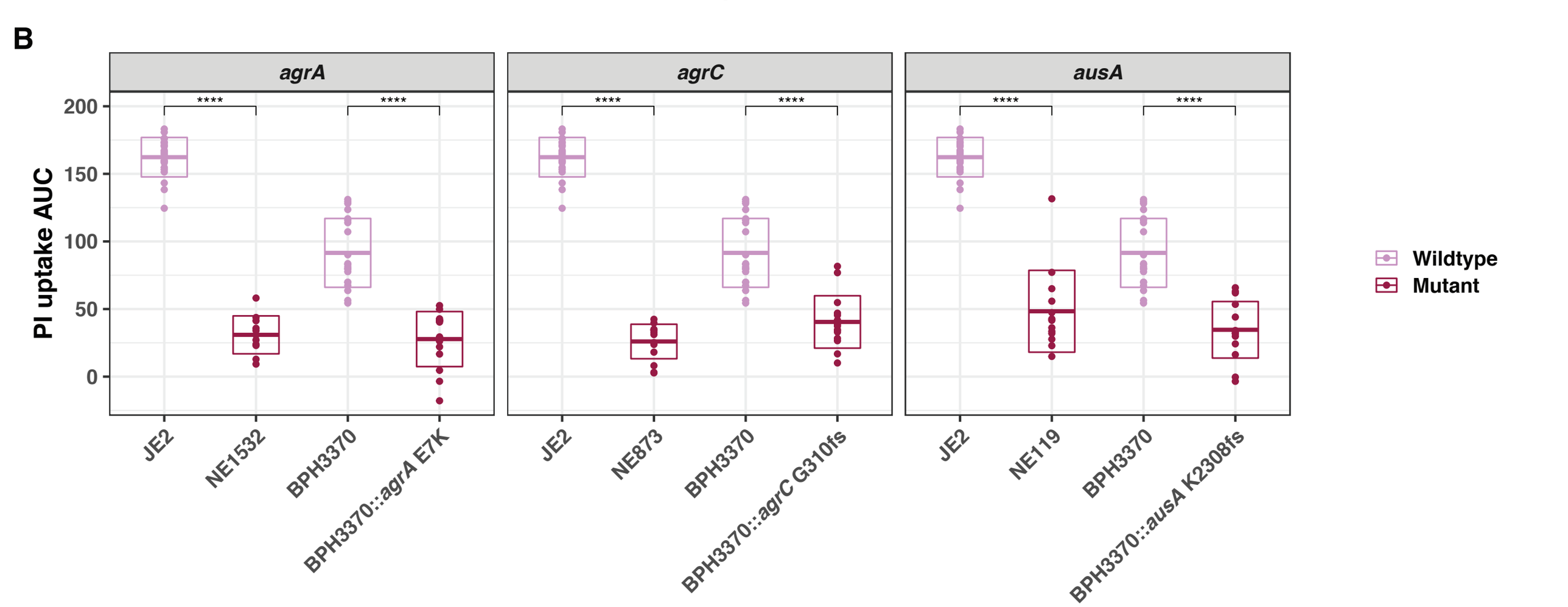

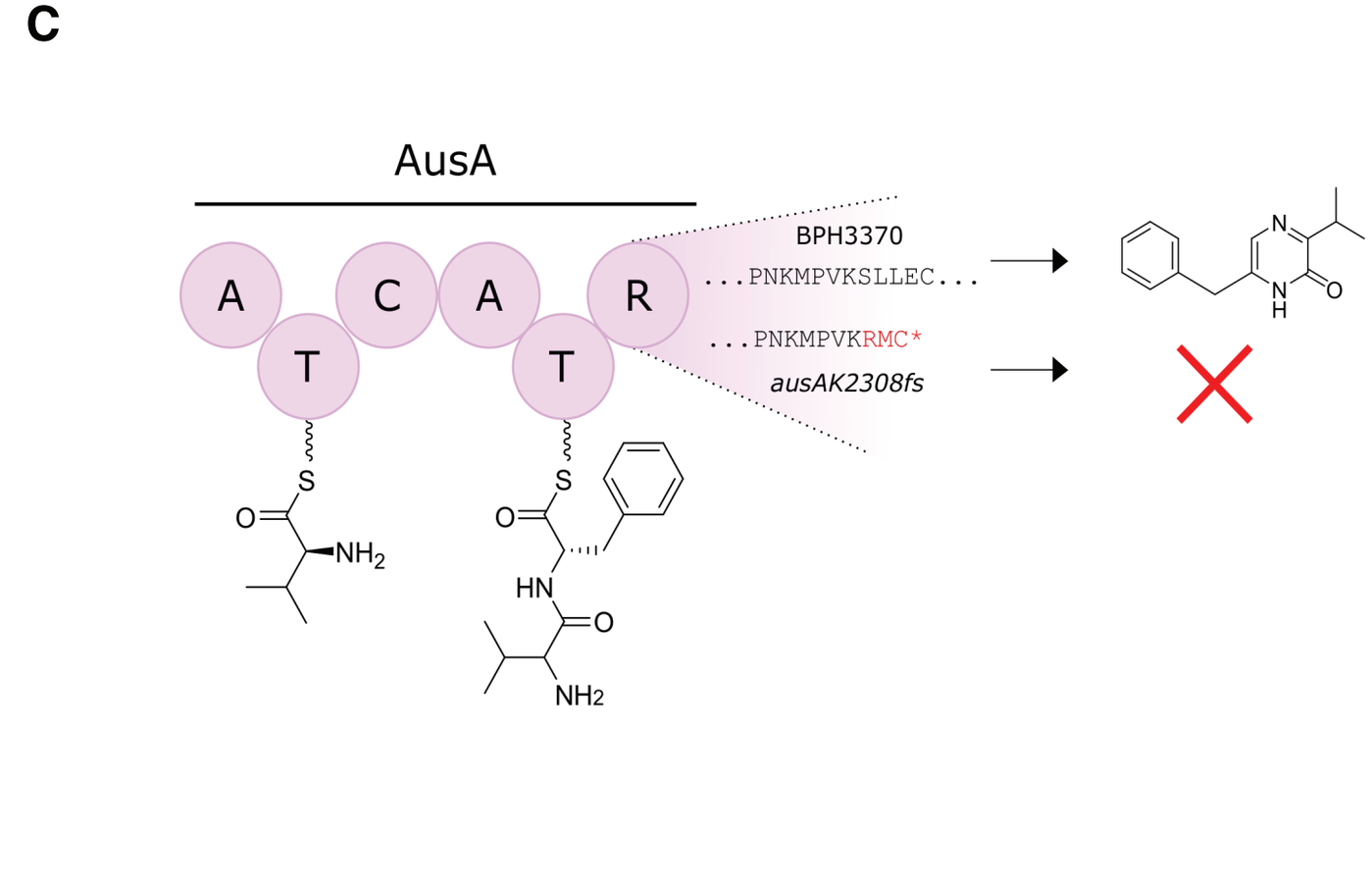

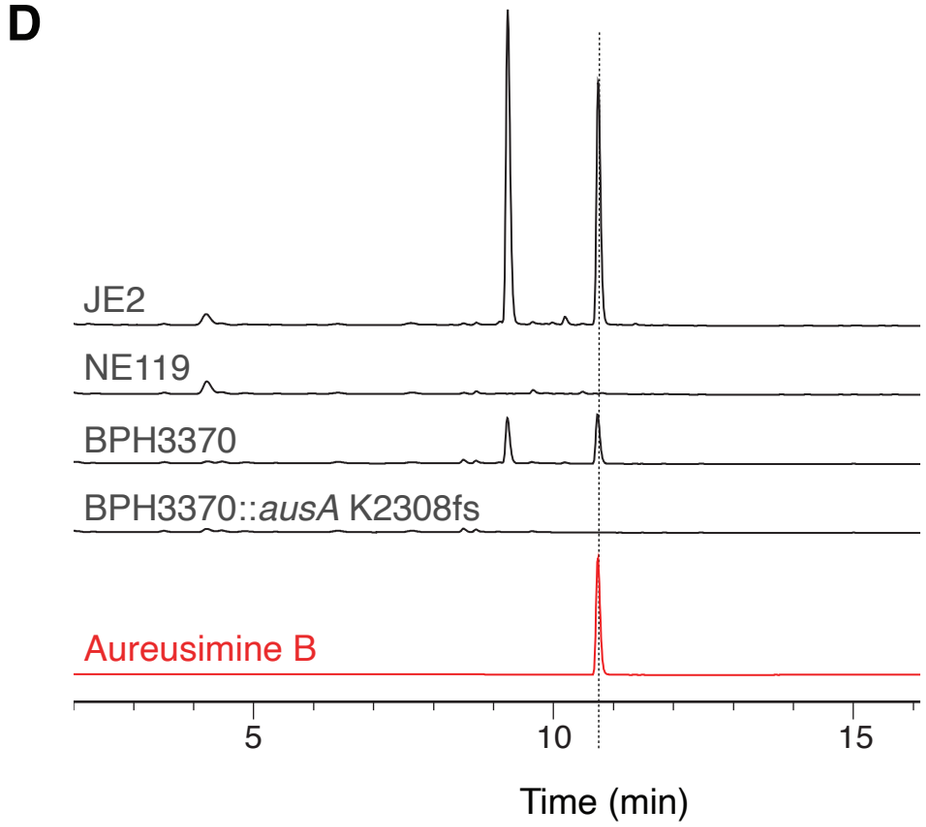

Figure 1—Supplementary figure 1.

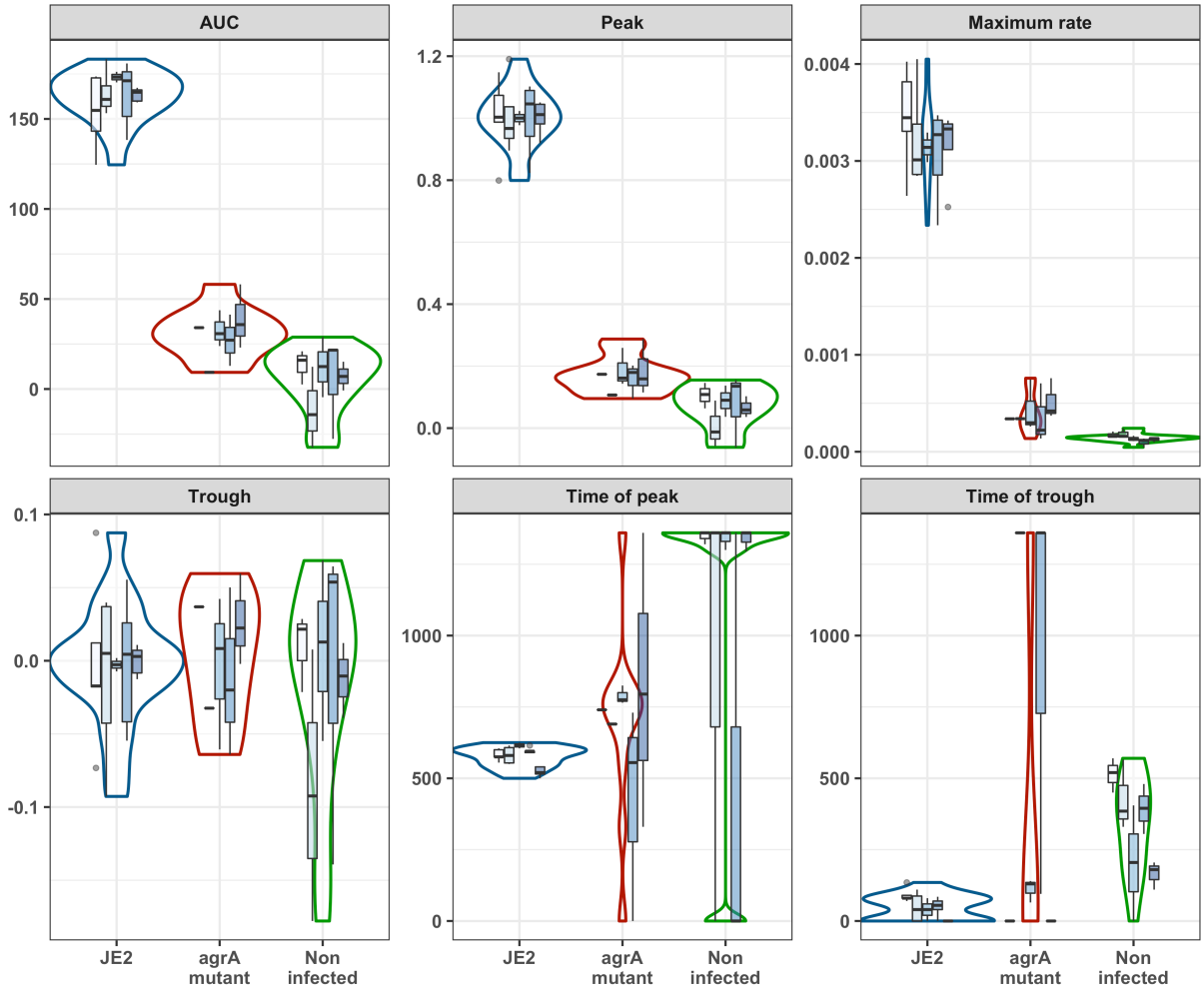

Summary of all PI uptake parameters across five experimental replicates
Violin plots represent the density distribution of all five replicates and the nested box plots show the distribution of within plate replicates (3-5 technical replicates per plate replicate) for t area-under-the-curve representing the total of PI uptake over time [AUC], peak PI uptake [μ^{max}], the maximum rate in PI uptake [r^{max}], the time to r^{max} [$t(r^{max})$]), trough and time to trough. Error bars represent the standard deviation across the five independent experiments.

Figure 4—Supplementary figure 1.

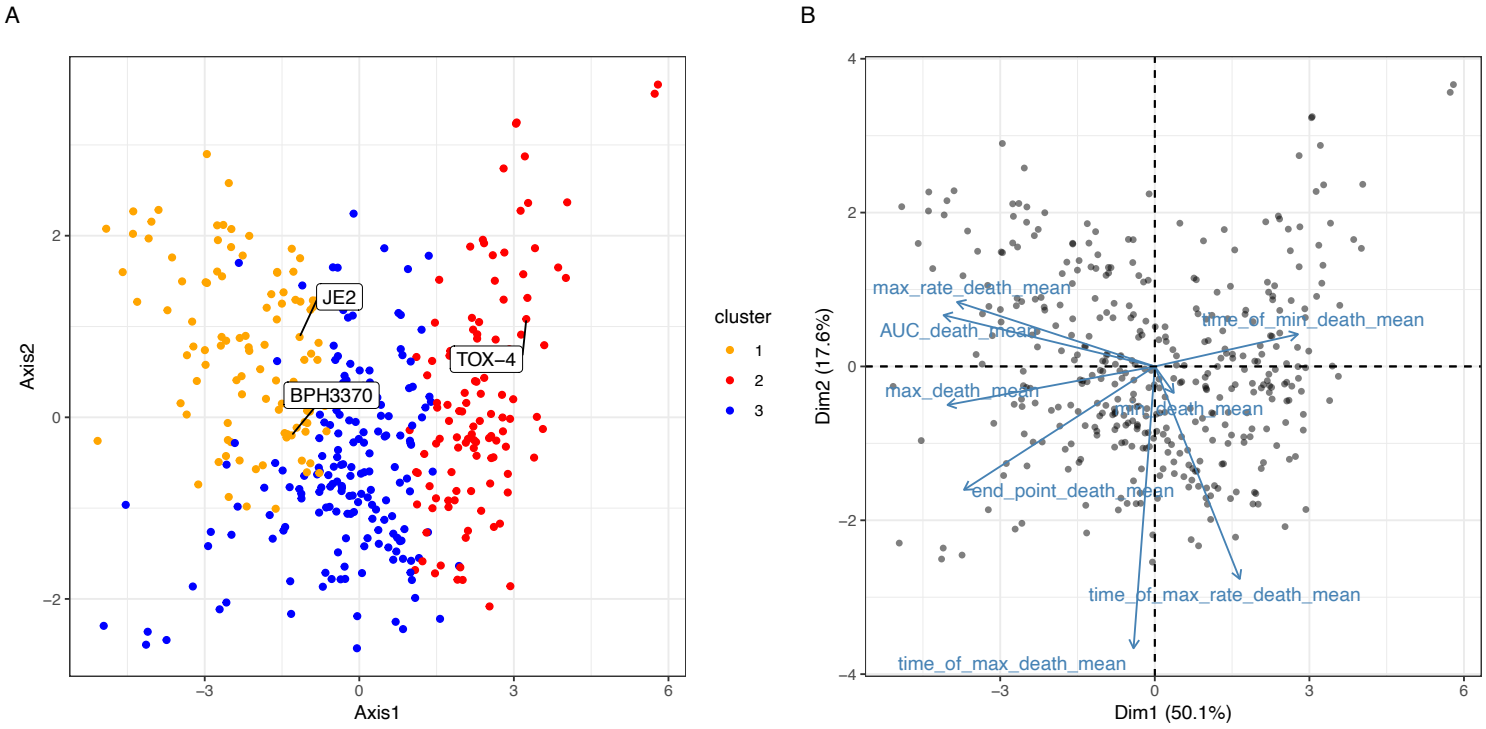

Principal component analysis of mean value of PI uptake parameters.
(A) Scatter plot of the first two principal components, representing 67% of the variance. Dots are coloured based on the clustering obtained from the proximity matrix of the unsupervised model.
(B) Loading plot showing the contribution of each PI uptake parameter to the first two PCA components.

Figure 4—Supplementary figure 2.

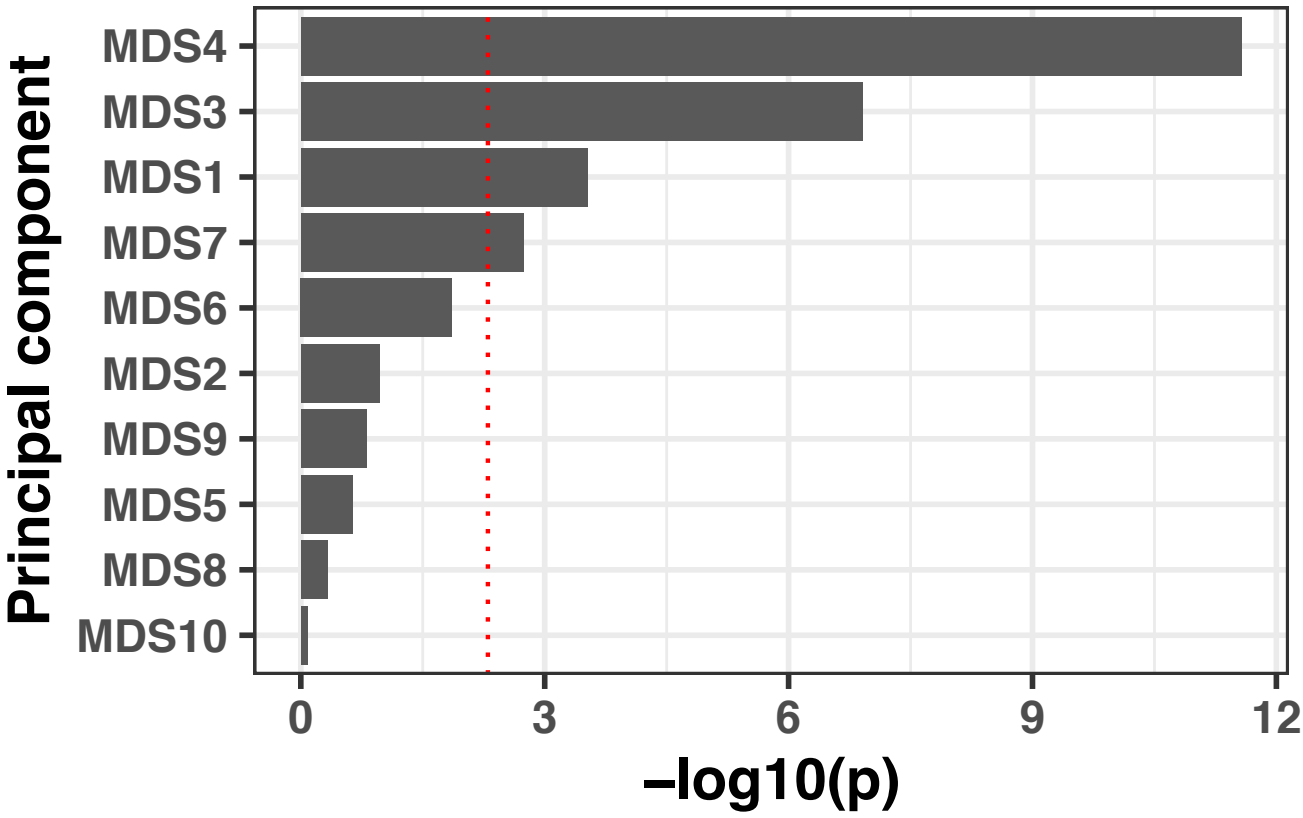

Lineage effects of cytotoxicity (AUC of PI uptake).
Lineages were calculated using multidimensional scaling on a distance matrix generated by Mash. The association with the phenotype was calculated by computing the fixed effect of the first 10 components by linear regression.

Figure 4—Supplementary figure 3.

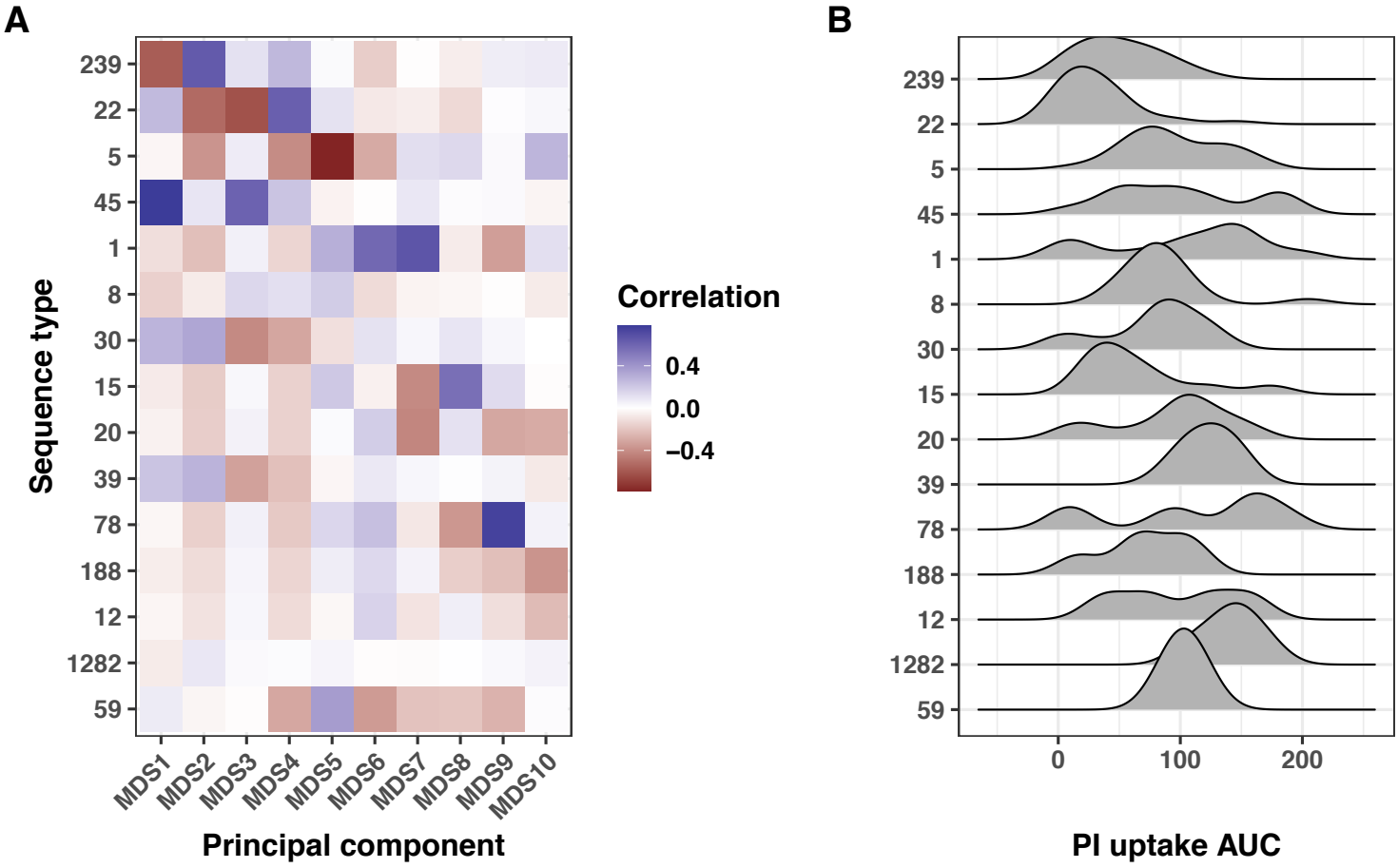

Interplay between multidimensional scaling (MDS) axes, sequence types and PI uptake.
(A) Heatmap showing the correlation between the first ten MDS axes and the fifteen most prevalent sequence types (ST). Here, MDS was applied to a genetic distance matrix calculated from Mash sketches (10,000 hashed k-mers per set). The correlations were calculated using the R package bugwas.
(B) Ridge plots depicting the PI uptake AUC distribution for the fifteen most prevalent STs.

Figure 6—Supplementary figure 1.

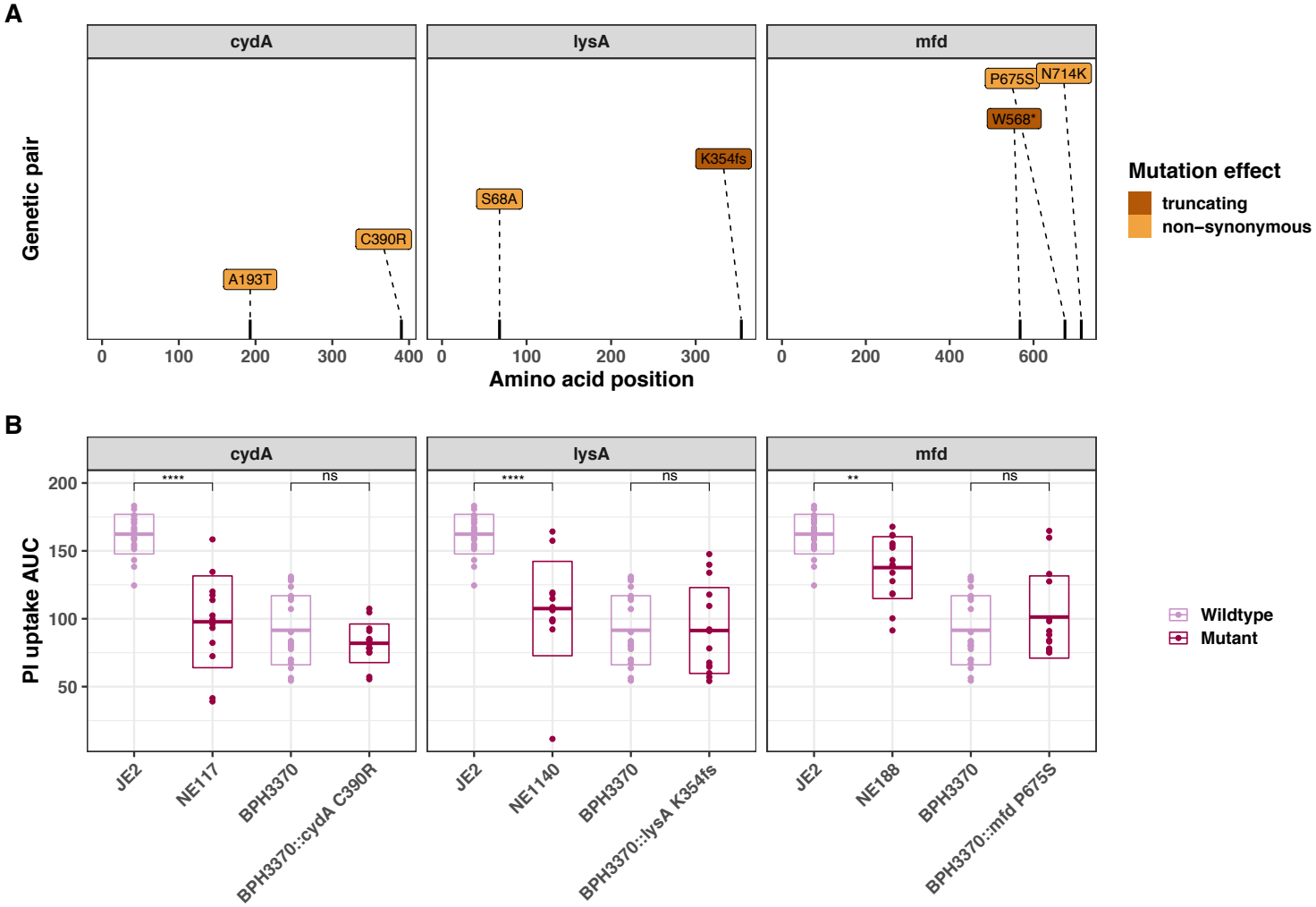

Introduction of convergent *cydA*, *lysA* and *mfd* mutations in the clinical isolate BPH3370 do not affect its intracellular cytotoxicity.

(A) Position and nature of convergent mutations identified in the genes *cydA*, *lysA* and *mfd*. For each gene, the amino acid position affected by mutations is shown on the x-axis for each gene. Convergent mutations causing a significant contrasting PI uptake phenotype is colored according to its consequence on protein function: non-synonymous (orange) and truncating (characterized by the introduction of a frameshift (fs) or a strop codon (*) (maroon).